







## Article

# A Multidisciplinary Approach for Groundwater Potential Mapping in a Fractured Semi-Arid Terrain (Kerdous Inlier, Western Anti-Atlas, Morocco)

Khalid Benjmel <sup>1,\*</sup> , Fouad Amraoui <sup>1</sup>, Ali Aydda <sup>2</sup> , Amine Tahiri <sup>1</sup>, Mohamed Yousif <sup>3</sup> , Biswajeet Pradhan <sup>4,5,6</sup> , Kamal Abdelrahman <sup>7</sup> , Mohammed S. Fnais <sup>7</sup> and Mohamed Abioui <sup>2,\*</sup> 

<sup>1</sup> Laboratory of Geosciences Applied to Engineering Development (GAIA), Faculty of Science Ain-Chock, Hassan II University of Casablanca, Maarif, Casablanca 20150, Morocco; amraoui\_f@hotmail.com (F.A.); tahiri.amine28@gmail.com (A.T.)

<sup>2</sup> Department of Earth Sciences, Faculty of Sciences, Ibn Zohr University, Agadir 80000, Morocco; a.aydda@uiz.ac.ma

<sup>3</sup> Desert Research Centre, Geology Department, El Matariya, Cairo 117753, Egypt; yousif\_mohamed80@daad-alumni.de

<sup>4</sup> Centre for Advanced Modelling and Geospatial Information Systems (CAMGIS), School of Civil and Environmental Engineering, Faculty of Engineering and IT, University of Technology Sydney, Sydney, NSW 2007, Australia; biswajeet.pradhan@uts.edu.au

<sup>5</sup> Center of Excellence for Climate Change Research, Department of Meteorology, King Abdulaziz University, Jeddah 21589, Saudi Arabia

<sup>6</sup> Earth Observation Centre, Institute of Climate Change, Universiti Kebangsaan Malaysia, Bangi 43600, Malaysia

<sup>7</sup> Department of Geology & Geophysics, College of Science, King Saud University, P.O. Box 2455, Riyadh 11451, Saudi Arabia; khassanein@ksu.edu.sa (K.A.); mfneis@ksu.edu.sa (M.S.F.)

\* Correspondence: khalid.benjmel-etu@etu.univh2c.ma (K.B.); m.abioui@uiz.ac.ma (M.A.)



**Citation:** Benjmel, K.; Amraoui, F.; Aydda, A.; Tahiri, A.; Yousif, M.; Pradhan, B.; Abdelrahman, K.; Fnais, M.S.; Abioui, M. A Multidisciplinary Approach for Groundwater Potential Mapping in a Fractured Semi-Arid Terrain (Kerdous Inlier, Western Anti-Atlas, Morocco). *Water* **2022**, *14*, 1553. <https://doi.org/10.3390/w14101553>

Academic Editor: Domenico Cicchella

Received: 29 March 2022

Accepted: 10 May 2022

Published: 12 May 2022

**Publisher's Note:** MDPI stays neutral with regard to jurisdictional claims in published maps and institutional affiliations.



**Copyright:** © 2022 by the authors. Licensee MDPI, Basel, Switzerland. This article is an open access article distributed under the terms and conditions of the Creative Commons Attribution (CC BY) license (<https://creativecommons.org/licenses/by/4.0/>).

**Abstract:** This study is focused on developing an approach for spatial mapping of groundwater by considering four types of factors (geological, topographical, hydrological, and climatic factors), and by using different bivariate statistical models, such as frequency ratio (FR) and Shannon's entropy (SE). The developed approach was applied in a fractured aquifer basin (Ameln Basin, Western Anti-Atlas, Morocco), to map the spatial variation of groundwater potential. Fifteen factors (15) influencing groundwater were considered in this study, including slope degree, slope aspect, elevation, topographic wetness index (TWI), slope length (LS), topographic position index (TPI), plane curvature, profile curvature, drainage density, lineament density, distance to rivers and fault network, normalized difference vegetation index (NDVI), lithology, and land surface temperature (LST). The potential maps produced were then classified into five classes to illustrate the spatial view of each potential class obtained. The predictive capacity of the frequency ratio and Shannon's entropy models was determined using two different methods, the first one based on the use of flow data from 49 boreholes drilled in the study area, to test and statistically calibrate the predictive capacity of each model. The results show that the percentage of positive water points corresponds to the most productive areas (high water flow) (42.86% and 30.61% for the FR and SE models, respectively). On the other hand, the low water flows are consistent with the predicted unfavorable areas for hydrogeological prospecting (4.08% for the FR model and 6.12% for the SE model). Additionally, the second validation method involves the integration of 7200 Hz apparent resistivity data to identify conductive zones that are groundwater circulation zones. The interpretation of the geophysical results shows that the high-potential zones match with low apparent resistivity zones, and therefore promising targets for hydrogeological investigation. The FR and SE models have proved very efficient for hydrogeological mapping at a fractured basement area and suggest that the northern and southern part of the study area, specifically the two major fault zones (Ameln Valley in the north, and the Tighmi-Tifermit Valley in the south) has an adequate availability of groundwater, whereas the central part, covering the localities of Tarçouat, Boutabi, Tililan, and Ighalen, presents a scarcity of groundwater. The trend histogram of the evolution of positive water points according to each potentiality class obtained suggests that the FR model was more accurate than the SE model.

in predicting the potential groundwater areas. The results suggest that the proposed approach is very important for hydrogeological mapping of fractured aquifers, and the resulting maps can be helpful to managers and planners to generate groundwater development plans and attenuate the consequences of future drought.

**Keywords:** Ameln Basin; frequency ratio; Shannon's entropy; GIS; remote sensing

## 1. Introduction

Water is a precious and vital resource around the world. It is a resource that is becoming increasingly scarce in many parts of the world. Moreover, the request for drinking water to satisfy the water needs of the population is increasingly strong. Since Morocco is one of the North African countries that is mainly characterized by its arid to semi-arid bioclimatic stage, the country is heading for a water crisis mainly caused by its inefficient water resources management policy, spatiotemporal water irregularity, and drought caused by climate change [1–9]. Groundwater resources in the basement zone represent a major resource for rural populations in the mountainous areas of Morocco. Since surface water is not perennial, groundwater conditions the food security of these populations [10–14]. Basement aquifers are generally characterized by a geographically irregularly distributed water resource. Access to this groundwater for domestic use is achieved by drilling wells or boreholes capable of providing quality water and sustainability over time. These wells should be located in aquifers with significant storage and/or recharge. The scarce groundwater in the Kerdous crystalline basement (Ameln Basin, Western Anti-Atlas, Morocco) developed in a fractured environment and is distributed illegally throughout the basin. Their sustainable management represents a major socio-economic development challenge for the region [6,15–17]. This basin is located in a complex geological setting where the Kerdous crystalline basement formations are dominant. In such environments, groundwater resources can hardly supply the increasing demand induced by the demographic evolution of rural populations [18–20]. Therefore, the identification of an appropriate method for groundwater management and prediction at regional and local levels is necessary, using efficient, accurate, advanced, and cost-effective modeling methods such as remote sensing and geographic information systems [21–23] because, generally, conventional approaches (geophysical, hydrochemical, etc.) are expensive, less accurate, and take too much time [24,25]. Remote sensing (RS) and geographic information systems (GIS) are widely applied in water resources research. GIS is a useful tool that has some advantages for acquiring, storing, analyzing, modeling, archiving, and sharing geographic information to manage a massive quantity of spatial data used in the decision-making process [26]; on the other hand, remote sensing facilitates a wide range of studies and a synoptic view of spatio-temporal distribution observations in a better and faster assessment [27]. Exploration using RS and GIS integration has recently attracted attention as a cost-effective and efficient method [28,29]. In this work, groundwater potential zones were delineated by integrating various thematic maps (NDVI, LST, and lineament density) generated from remote-sensing data (Landsat 8 Oli); on the other hand, other criteria such as slope, slope aspect, elevation, topographic wetness index (TWI), slope length (LS), topographic position index (TPI), plane curvature, profile curvature, drainage density, distance to rivers, and fault network were plotted in a GIS environment. There are several hydrogeological mapping methods, such as the analytical hierarchy process (AHP) [6,30–32], analytical network process (ANP) [33], multi-influence factor analysis (MIF) [34,35], boosted regression tree [36], advanced machine learning algorithms [37], weighted overlay analysis [38], frequency ratio model [39–42], and Shannon's entropy models [42–44] were used to identify groundwater exploration areas and artificial recharge sites. The application of the frequency ratio and Shannon's entropy model has not yet been used in Morocco, especially for hydrogeological mapping in an environment that is characterized by fracture porosity [45–47]. FR is a simple

bivariate statistical tool to calculate the probabilistic relationship between independent and dependent variables; it is a very simple and flexible technique to delineate potential areas of discontinuous aquifers [48,49]. In contrast, Shannon's entropy model represents the average unpredictability of a random variable. Groundwater potential entropy refers to the extent to which various controlling groundwater occurrences influence groundwater productivity. References [41,44] conducted a comparative study between FR and entropy index, for mapping the potential of qanats in the Moghan watershed, Iran. They concluded that both techniques are effective for delineating areas with similar potential and climate as compared to our case study. The main objective of this study is to delineate the groundwater availability of the aquifer system in the study area using the FR and SE models. The resulting groundwater potential maps will be useful for water resource managers to efficiently guide future drilling and, consequently, sustainably manage groundwater resources.

## 2. Study Area

The Ameln Basin is located in the northern part of the Tiznit district and covers an area of 712 km<sup>2</sup> with an average altitude of 1324 m (Figure 1). From a climatic point of view, the study area is characterized by a semi-arid climate, where the minimum and the maximum temperatures are 2 and 41 °C, respectively, and the average annual precipitation is about 287 mm (Figure 2). The most current land uses in this region are the building areas, almond trees, and argan trees, with an abundance of skeletal soils and superficial rock. They are classified as soils of lesser quality; consequently, the agricultural production potential of these soils is low and the forest cover remains low throughout the territory. The hydrographic network in the study area is characterized by a strong seasonal and interannual irregularity of the flows. Floods are often violent and rapid. The rivers are not perennial and dry most of the year because of the aridity of the region's climate, which makes the exploitation of these water resources difficult. From a geologic point of view, the study area is part of the Anti-Atlas (AA) belt of southern Morocco that is located at the northern boundary of the West African Craton (WAC) (Figure 3a). The AA belt corresponds to a broad mountain chain following the direction ENE–WSW and it is parallel to the High-Atlas belt. The contact between the aforementioned belts is marked by the southern Atlasic Fault. The Precambrian terrain (old units) outcrops as “inliers” that are distributed along two major faults zones (the southern Atlasic Fault and the Anti-Atlas major fault) (Figure 3b) [50–61]. The Kerdous inlier, where the study area is located, is the largest one in the western Anti-Atlas. The age of the units forming this terrain range from Paleoproterozoic to Cambrian, where they are distinguished from each other by tectonics unconformities [53,62–65]. The Paleoproterozoic of the Ameln Basin includes a weakly metamorphic schist series: green-schists, sericite-schists, mica-schists, basic volcanic rocks (gabbro and dolerites), and granites that crosscut them all, forming a metamorphism contact. The tectonic directions recorded in these old formations are E–W and ESE–WNW [62,64–66]. The Upper Neoproterozoic formations include thick quartzite mostly corresponding to the major ridges (Jbel Lkst of Kerdous), basic volcanic rocks (gabbros and dolerites), and schists with conglomerates and basic vulcanites. After successive volcanic events, the Anti-Atlas domain recognized a great transgression from the west forming the Lower Paleozoic cover that consists of a transgressive limestone or dolomitic level [67]. The Quaternary deposits consist of alluvial deposits that are forming the small generalized aquifers along the major valleys in the study area (Figure 4).

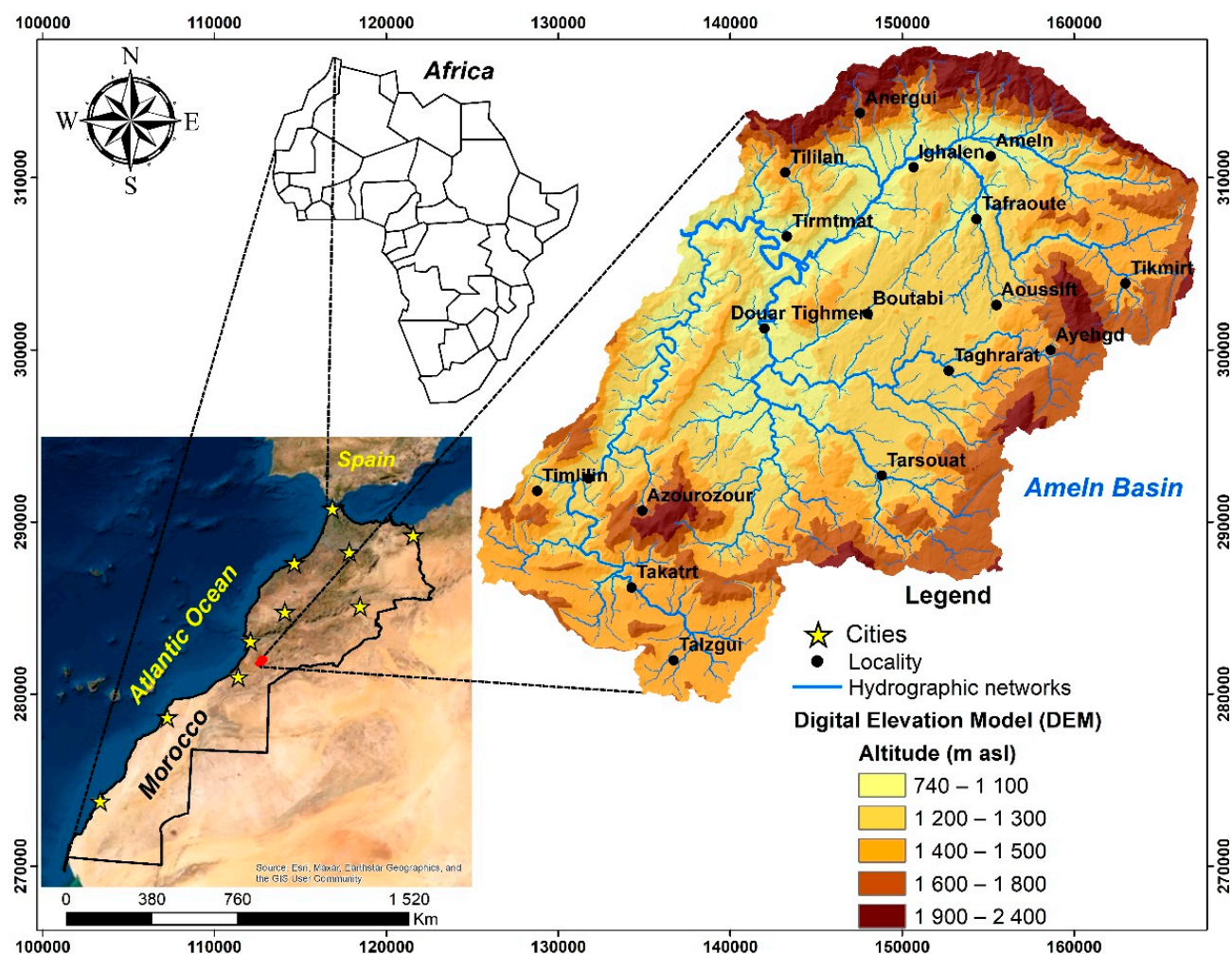


Figure 1. Geographic location of the Ameln Basin.

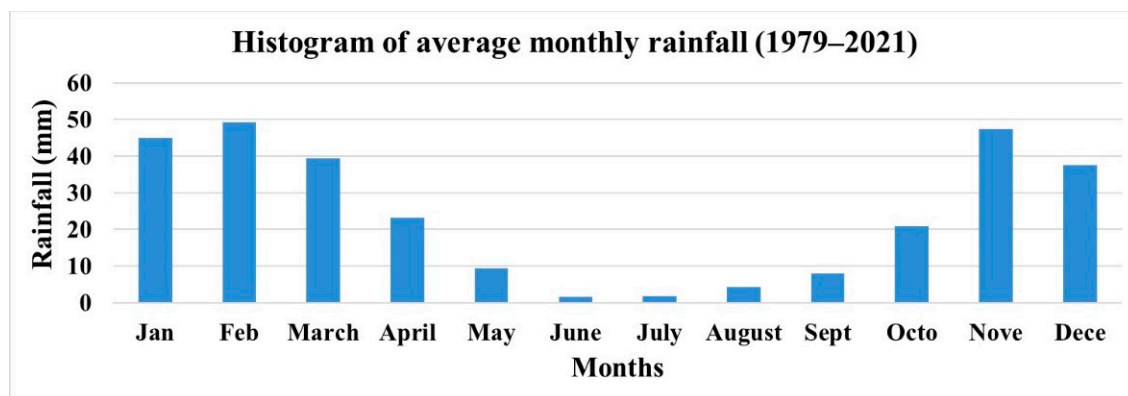


Figure 2. Histogram of the average monthly rainfall at Taфраout during (1979–2021) (According to the Souss-Massa Hydraulic Basin Agency).



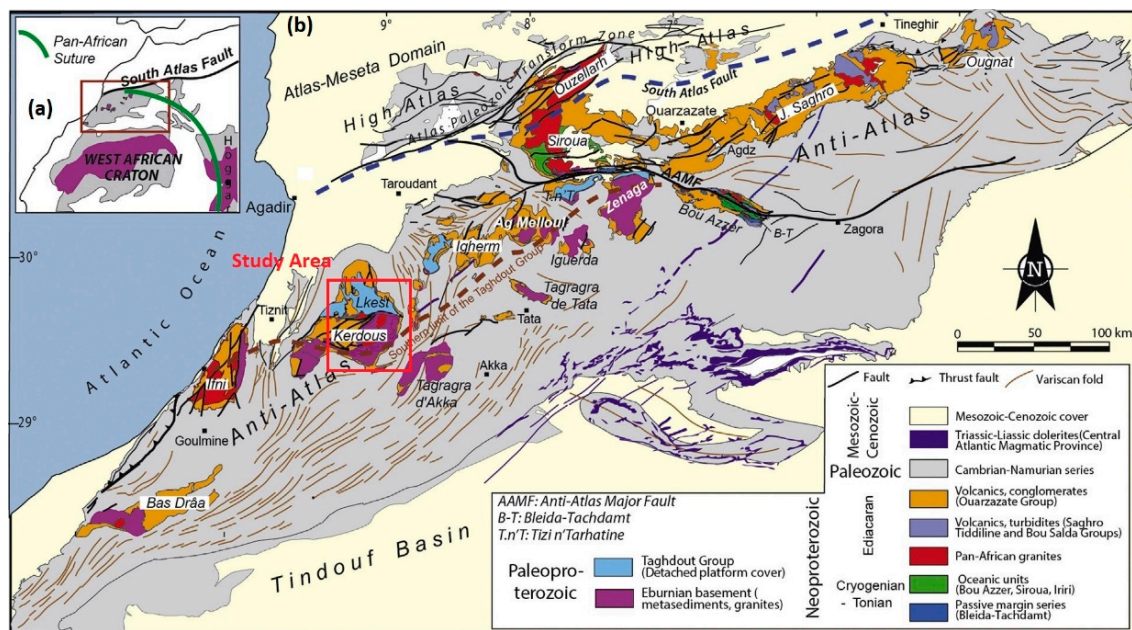


Figure 3. (a) The Anti-Atlas belt at the northern boundary of the West African Craton; (b) geological map of the Anti-Atlas belt, modified after [60,61].

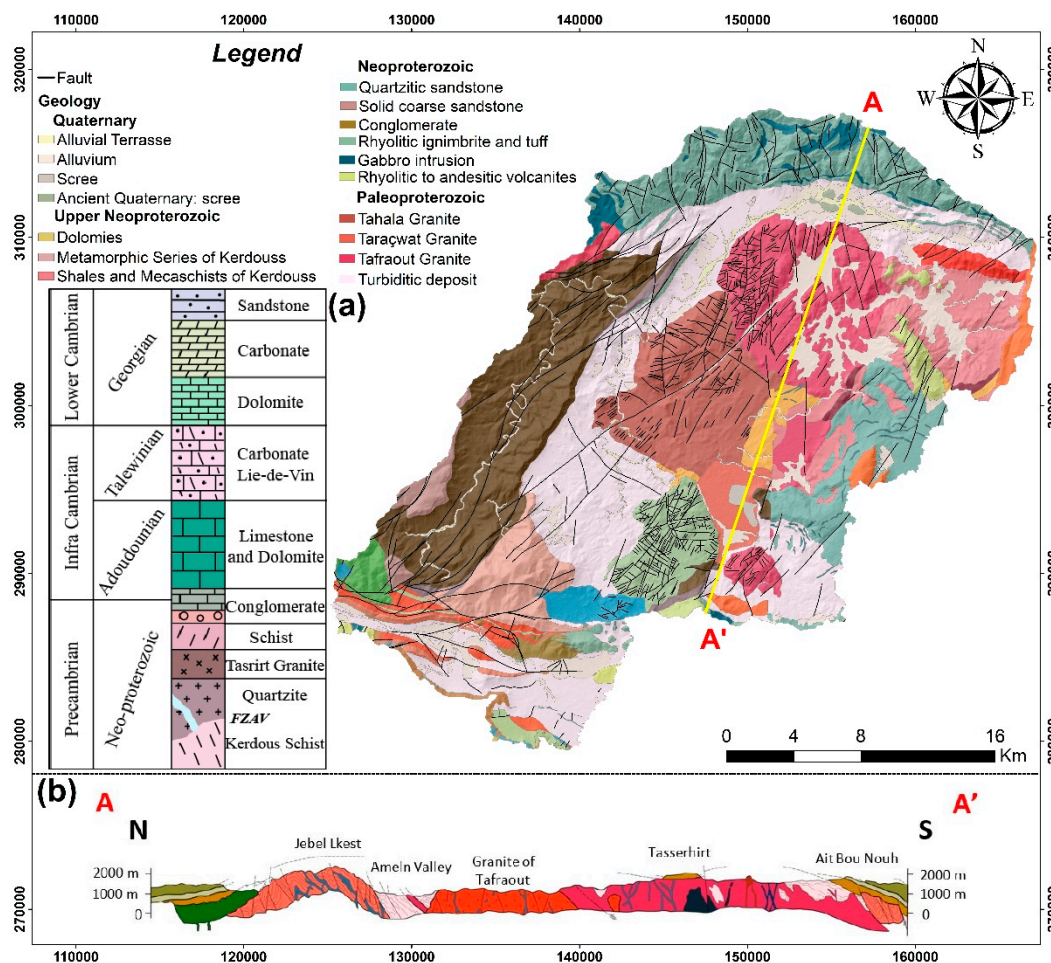
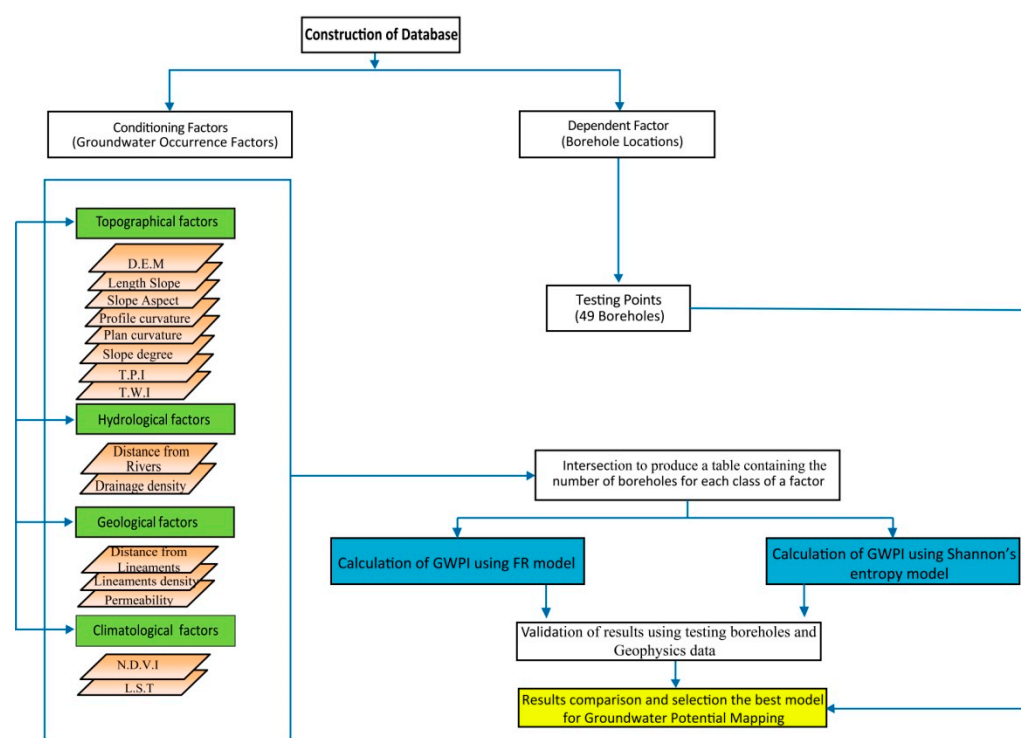


Figure 4. Geological map of the Ameln Basin. (a) Generalized lithostratigraphic column for the Kerdous inlier (modified after [60,61]); (b) geological section of the Ameln Basin.

### 3. Materials and Methods

#### 3.1. GIS Applications

In this study, to delineate the groundwater potential areas in the Ameln Basin, several GIS-based techniques were used, including numerical, cartographic, and geostatistical techniques. The methodology proposed for modeling aquifer productivity involves four steps: (1) preparation of data recorded from boreholes in the study area, (2) influencing factors data collection and spatial database preparation, (3) productive zones evaluation via the relationship between borehole data and influencing factors, and (4) results from validation and interpretation. The geospatial data were achieved using ArcGIS 10.4.1 software and the weights generation for the groundwater exploration factors and the associated functions were computed using Microsoft Excel. The validation of results was prepared as a histogram showing the productivity of each obtained groundwater potential class. The final map of the groundwater potentiality was achieved by multiplying each factor with its weight using a raster calculation tool in ArcGIS 10.4.1 software. Figure 5 shows the methodology applied in this study.



**Figure 5.** Flow chart of the methodology used in this study.

#### 3.2. Groundwater Occurrence Factors

In general, mapping groundwater potentiality depends on a variety of conditioning factors, which depend on data available in the study area [68]. In the present study, 15 groundwater influencing factors were used, which are grouped into four categories: topographic, hydrological, geological, and climatologic factors. The integration of these factors in a GIS-based model is anticipated to be an effective tool for predicting groundwater resource potentiality in the whole study area.

##### 3.2.1. Topographic Factors

Topographic factors, including slope degree, slope aspect, elevation, topographic wetness index (TWI), slope length (LS), topographic position index (TPI), plane curvature, and profile curvature, are considered essential to the spatial variation of surface water infiltration conditions. In this study, the topographic factors were prepared, in the ArcGIS platform, as individual maps from a digital elevation model (DEM) of 12.5 m of spatial

resolution that was collected free of charge from the Alaska satellite facility site. Among the topographic factors, the slope is considered an important one for identifying suitable locations for surface water infiltration, where low slope areas correspond to an area with low surface runoff and high percolation rates, while high slope areas indicate areas with high and rapid runoff [69]. The slope aspect identifies the downslope direction of the maximum rate of change in value from each pixel to its neighbors [70]. The slope aspect strongly controls the hydrological parameters, like evapotranspiration, precipitation direction, and weather process, especially in dry and arid areas without vegetation cover [71]. The elevation (altitude) is the height of an object above sea level. The elevation impacts the climate conditions that affect soil infiltration degree, vegetation type, and groundwater occurrence [49,72]. The high altitudes indicate areas with rapid and high runoff, while the lower altitudes indicate high surface water recharge and then high water infiltration [73]. The topographic wetness index (TWI) is an index used to describe spatial humidity models and explain the effects of the topographic conditions on them [74]. TWI affects runoff movement and accumulation [75]. TWI can be calculated using the following equation:

$$TWI = \left( \frac{As}{\tan \beta} \right) \quad (1)$$

where  $As$  is the cumulative surface of the ascending slope and  $\beta$  is the slope gradient.

Slope length (LS) is the combination of slope (S) and slope length (L). LS can be derived from the universal soil loss equation (USLE), which is mostly used to estimate the water erosion and transported sediments rates [75]. Moore and Burch [76] reported an equation to calculate the LS factor as below:

$$LS = \left( \frac{Bs}{22.13} \right)^{0.6} \left( \frac{\sin \beta}{0.0896} \right)^{1.3} \quad (2)$$

where  $Bs$  is the specific catchment area ( $m^2$ ) and  $\beta$  is the local slope gradient (degree).

The topographic position index (TPI) is an index used to analyze the topographic landscape units in the upper, middle, and lower portions of the watershed [77]. TPI evaluates the elevation of a pixel and the average elevation of pixels around it using the following Equation (3):

$$TPI = M0 - \sum_{n=1} \frac{Mn}{n} \quad (3)$$

where  $M0$  is the elevation of the point (pixel) under evaluation,  $Mn$  is the elevation of grid, and  $n$  is the total number of surrounding pixels used for evaluation. Curvature refers to the morphology of the topography and consists of three parameters: profile, plane, and a combination of both. Profile curvature and plane curvature mainly affect the acceleration and deceleration of flows, as well as the convergence and divergence of flows [44].

### 3.2.2. Hydrological Factors

In general, to estimate surface water flow and to determine groundwater infiltration, hydrological factors like drainage density and distance from the river are to be taken into account. The drainage is controlled by the nature, structure, and lithology of the bedrock, the soil's capacity to infiltrate, type of vegetation, and slope angle [68,73]. The drainage density is the ratio of the total length of streams per unit of watershed area [78], as expressed in the following equation:

$$Dd = \frac{\sum Li}{A} \quad (4)$$

where  $Dd$  is drainage density ( $km^{-1}$ ),  $\sum Li$  is the total length of streams per unit (km), and  $A$  is an area ( $km^2$ ).

### 3.2.3. Geological Factors

Lithology is considered a crucial factor controlling aquifer porosity and permeability [68,79]. In addition, lineaments are considered an important geological factor and are linear or curvilinear structures often associated with various geomorphic features or tectonic structures. The orientation is not the only parameter characterizing a lineament network, but its density and connectivity are essential [80]. Lineament density is often used as a hydrodynamic indicator for groundwater resources functionality and determination of productive areas [6,68]. Furthermore, the distance from lineaments is considered an important factor to determine the hydrogeological interest areas, which are generally very close to these structures [6]. In this study, the lithology map of the study area was prepared from several geological maps (scale 1:50,000) through digitalization in the ArcGIS platform. On the other hand, the lineaments map was prepared by applying Sobel directional filtering on satellite images acquired by Landsat 8 OLI on 29 October 2020. They used satellite data collected free of charge from the US Geological Survey (USGS). First, several processing steps were applied to the collected data in image-processing software (ENVI 5) to extract the lineaments, including radiometric calibration and atmospheric correction using fast line-of-sight atmospheric analysis of spectral hypercubes (FLAASH) model, and transformation by applying principal component analysis (PCA). Afterward, the automatic lineaments extraction was achieved by applying different combinations of values for each parameter of the LINE module in Geomatica software. Then, the obtained map was verified using a faults map that was extracted from geological maps of the study area.

### 3.2.4. Climatological Factors

Climatological factors are most important to identify the areas of hydrogeological importance [81,82]. A normalized difference vegetation index (NDVI) is usually used to estimate the spatiotemporal changes in vegetation distribution [81,82]. In general, the presence of vegetation cover reflects the presence of near-surface aquifers [41,83]. In this study, an NDVI map was prepared, from the same Landsat 8 OLI scene used for lineaments extraction, using the following equation:

$$NDVI = \frac{(\rho_{NIR} - \rho_R)}{(\rho_{NIR} + \rho_R)} \quad (5)$$

where  $\rho_{NIR}$  and  $\rho_R$  are spectral reflectance in the red and near-infrared, respectively.

Furthermore, the land surface temperature (LST) was mapped using the following equation:

$$LST = \frac{BT}{\left(1 + \left(\frac{0.00115 * BT}{1.4388}\right) * \ln(\epsilon)\right)} \quad (6)$$

where  $\epsilon$  and BT are emissivity and brightness temperature conversion, respectively, extracted from the thermal infrared bands (10 and 11) of the same Landsat scene imagery.

### 3.3. Modeling Techniques

This study is based on a combination of remote sensing (RS) and geographic information systems (GIS) to prepare the parameters controlling the availability of groundwater resources. Finally, weights were assigned for different thematic layers and their classes using statistical analysis and to calculate the groundwater potential index using the FR and SE models; the results were interpreted and validated by exploiting the hydrogeological and geophysical data to choose the most adequate model for hydrogeological exploration. Figure 6 shows the role of all the techniques incorporated in this study.



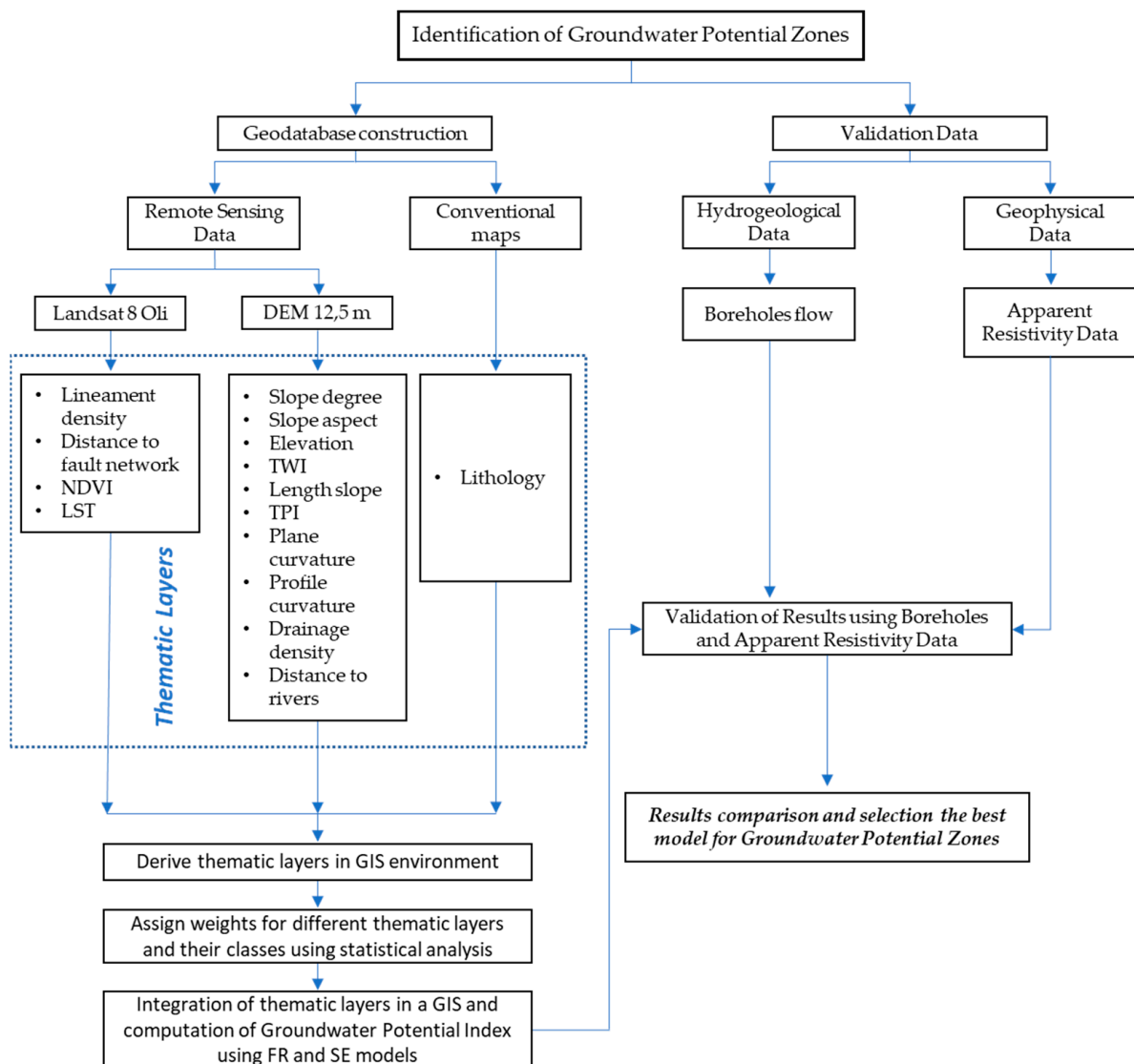


**Figure 6.** Flowchart shows the role of all spatial data and techniques incorporated in this study.

### 3.3.1. Frequency Ratio Model

The frequency ratio is a quantitative method popularly used to estimate the probability of occurrence and non-occurrence of a given attribute [84]. In this study, the frequency ratio model was used to determine the relationship between each borehole location and a class of the groundwater occurrence factor using Equation (7):

$$FR = \left( \frac{A/B}{C/D} \right) \quad (7)$$

where A is an area of a class of the factor influencing groundwater, B is a total area of the factor, C is a number of pixels in the class area of the factor, and D is a total number of pixels of the total study area. Moreover, the groundwater productivity based on the FR model was calculated using the equation in following [39,41,85]:

$$GWPI_{FR} = \sum_{i=1}^n FR_i \quad (8)$$

where  $FR_i$  is the frequency ratio of the factor and  $n$  is a total number of the used factors.

### 3.3.2. Shannon's Entropy Model

Entropy provides a measure of the uncertainty of a random variable system [86], where the groups are equally distributed within the system [87]. Precisely, the entropy model provides the extent of instability, disorder, disequilibrium, and uncertainty in a system [88]. Herein, the application of the entropy model consists of determining the occurrence factors impacting groundwater productivity. Therefore, the entropy value can be used to calculate the system weights index [85]. The information coefficient ( $V_j$ ) is the weight value of each occurrence-controlling factor [43,89]. The information coefficient ( $V_j$ ) can be calculated using the following Equations (9)–(14):

$$P_{ij} = FR = \frac{a}{b} \quad (9)$$

$$P_{ij} = \frac{P_{ij}}{\sum_{j=1}^{S_j} P_{ij}} \quad (10)$$

$$H_j = - \sum_{i=1}^{s_j} (P_{ij}) \log_2(P_{ij}), j = 1, \dots, n \quad (11)$$

$$H_{j\max} = \log_2 S_j \quad (12)$$

$$I_j = \frac{H_{j\max} - H_j}{H_{j\max}}, I = (0, 1), j = 1, \dots, n \quad (13)$$

$$V_j = I_j P_{ij} \quad (14)$$

The groundwater potential index based on the SE model (GWPI<sub>vj</sub>) was calculated using the equation below [43]:

$$GWPI_{vj} = \sum_{i=1}^n \frac{Z}{m_i} \times C \times V_j \quad (15)$$

where FR is frequency ratio,  $P_{ij}$  is a probability density,  $H_j$  and  $H_{j\max}$  are entropy values,  $S_j$  is a number of classes,  $I_j$  is information coefficient,  $V_j$  is the weight value of the factor,  $i$  is a number of particular factors maps,  $Z$  is a number of classes in the factor map of the whole classes,  $m_i$  is a number of classes in the particular factor map,  $C$  is the class value after secondary classification, and  $V_j$  is the weight value of the factor.

## 4. Results and Discussion

### 4.1. Conditioning Factors

The slope and altitude maps show that the low slope areas correspond to the central and southern parts of the study area, and to the valley draining the Ameln Basin, while the high slope areas correspond to the quartzites of Jbel Lkest, sandstones of Tizoughrane, and granitic arenas of Tafraout (Figure 7a,b). In general, due to slow runoff flows in the Ameln Valley, south of Ait Ouafqa and north of the Tarçouat areas located in the north of the study area are more suitable for groundwater recharge. The slope aspect map shows that the valleys (like Ameln and Oumaghous) characterized by downward-direction slopes oriented to the western side are considered areas of hydrogeological interest (Figure 8a). In general, the boreholes were installed along these valleys because of the descending underflows from the Precambrian massifs.

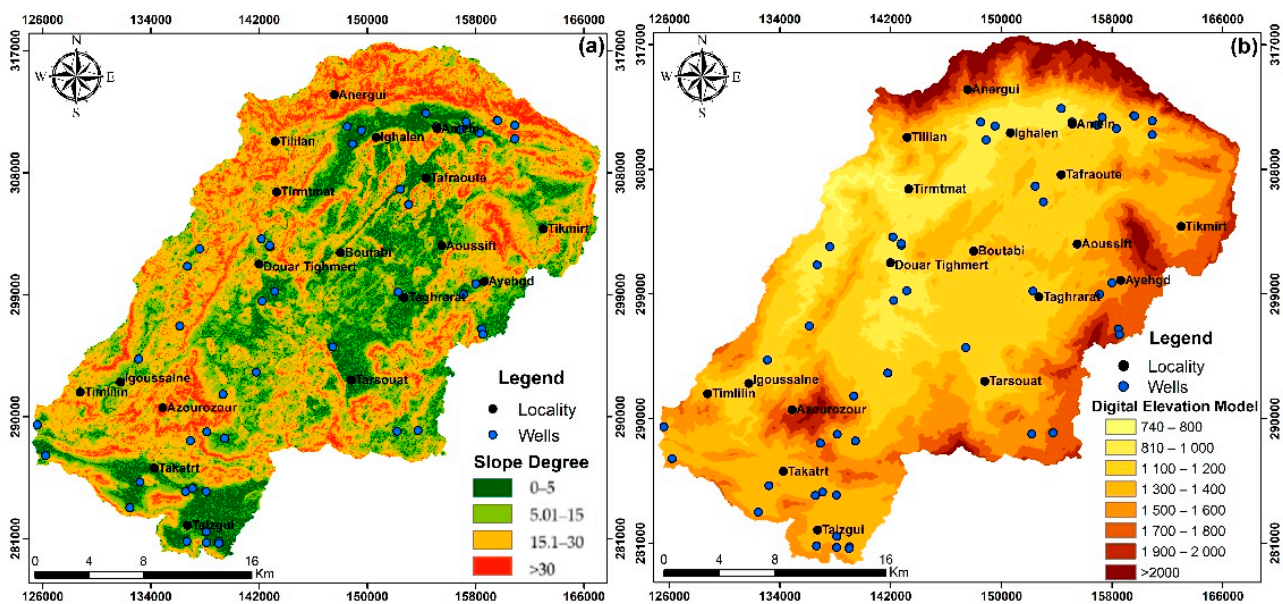


Figure 7. Topographical factors influencing groundwater. (a) Slope degree; (b) Altitude.

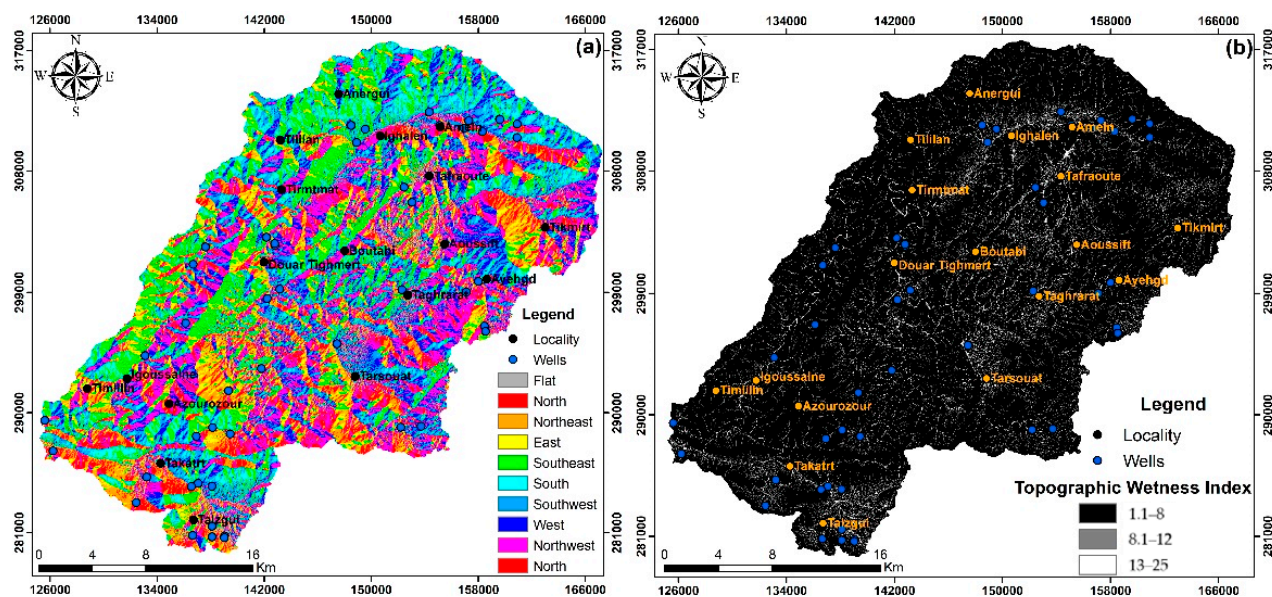
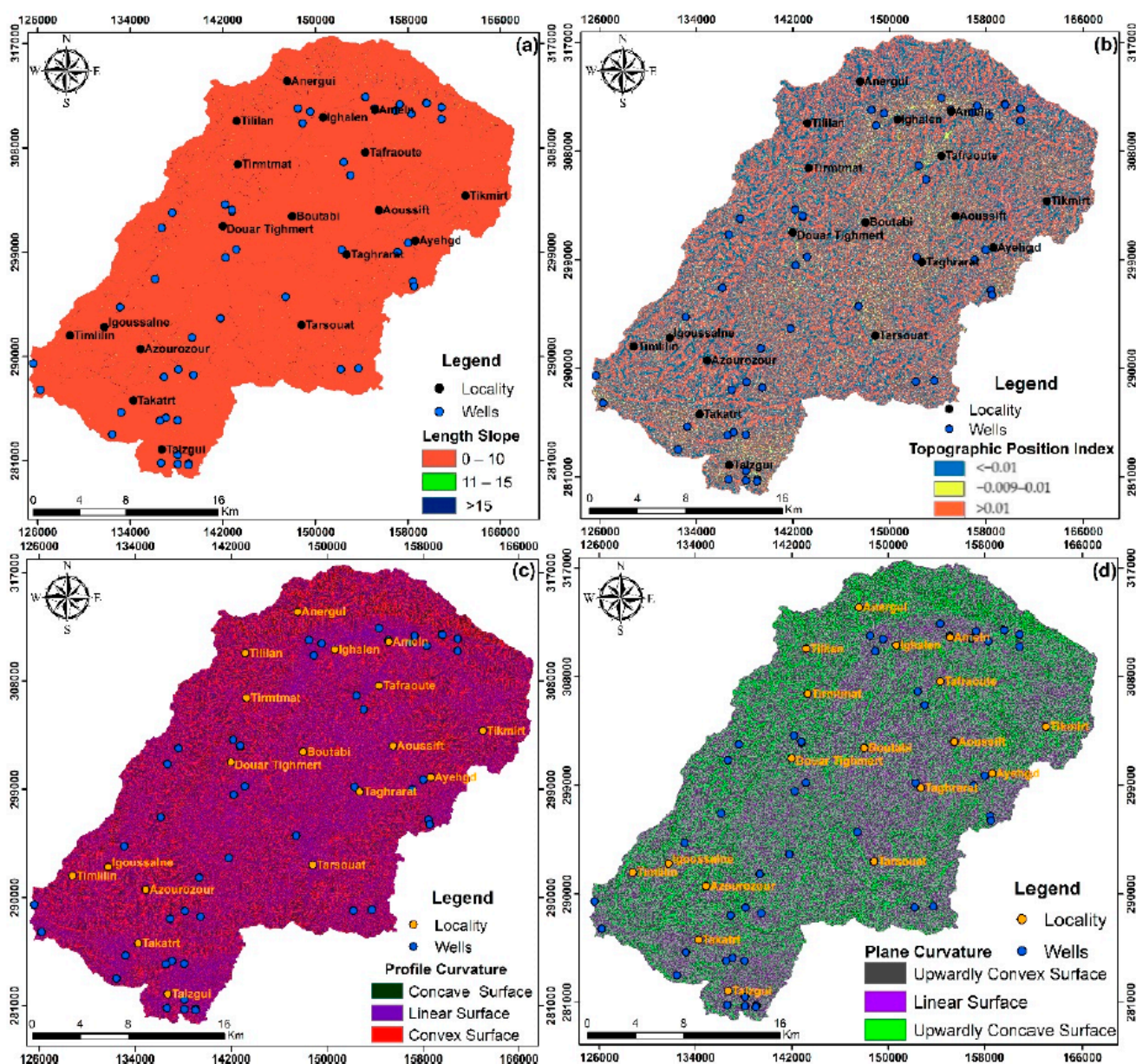


Figure 8. Topographical factors influencing groundwater. (a) Slope aspect; (b) Topographic wetness index.

The topographic wetness index (TWI) map shows that the TWI high values correspond to the valley areas (Ameln Valley and Assif Oumaghous) and to the hydrographic network areas that have intense ramifications (Figure 8b). These results prove that the TWI factor is an indicator of possible water drainage. The analysis of the obtained slope length (LS) map reveals that the LS high values correspond to the areas of high altitude (reliefs, like Jbel Lkest, Jbel Azourozour, and Jbel Ayehgd, while the low values of LS correspond to the low altitudes (Figure 9a). In general, the LS low values are more exposed to water recharge. The high TPI values correspond to the northern part of the Ameln Basin (Jbel Lkest quartzites), while the low TPI values correspond to the low altitude areas (Ameln and Oumaghous valleys) and TPI values close to zero correspond to the flatlands (Figure 9b).





**Figure 9.** Topographical factors influencing groundwater. (a) Length slope; (b) Topographic position index; (c) Profile curvature; (d) Plan curvature.

The idea behind using the profile curvature and plane curvature factors is to highlight different aspects of the ground surface shape. In general, profile curvature has paralleled the slope and indicates the direction of the maximum slope. The profile curvature affects the acceleration and deceleration of the water flow at the surface (Figure 9c). Indeed, the profile curvature negative values indicate that the surface is convex, causing dispersion of water. In contrast, the positive profile curvature values indicate that the surface is concave upward, favoring water stagnation and, then, increasing the water infiltration rate. On the other hand, the plane curvature refers to the convergence and divergence of water flow at the surface (Figure 9d). The plane curvature positive values indicate that the surface is a convex causing divergence of surface flows and a consequent loss of the surface water. On the contrary, the plane curvature negative values indicate that the surface is laterally concave causing convergence of the surface flows, which favors water reassembly toward zones favorable to its stagnation.

In our study area, the suitable areas for water stagnation correspond to the contact area between the great reliefs (quartzite formations of Jbel Lkest and granitic outcrops of



Precambrian age) and great valleys of Quaternary fillings. In general, the high drainage density decreases infiltration and increases surface runoff and is, therefore, not suitable for groundwater development [90], which means that drainage density is an inverse function of permeability. In our study area, the high values of runoff correspond to the Ameln Valley, Assif Idawsmal, and Assif Oumaghouz (Figure 10a). Moreover, the criterion distance from river networks had been considered an important factor in hydrogeological research, especially for arid areas, because the local alluvial aquifers usually prospect in areas near the rivers [6]. The obtained results reveal that the areas close to the rivers (200 m) characterized by a thick alluvial level (very permeable formations) are the most promising for water infiltration, while it seems difficult to find water resources in the areas far away from the rivers (distance > 500 m) (Figure 10b).

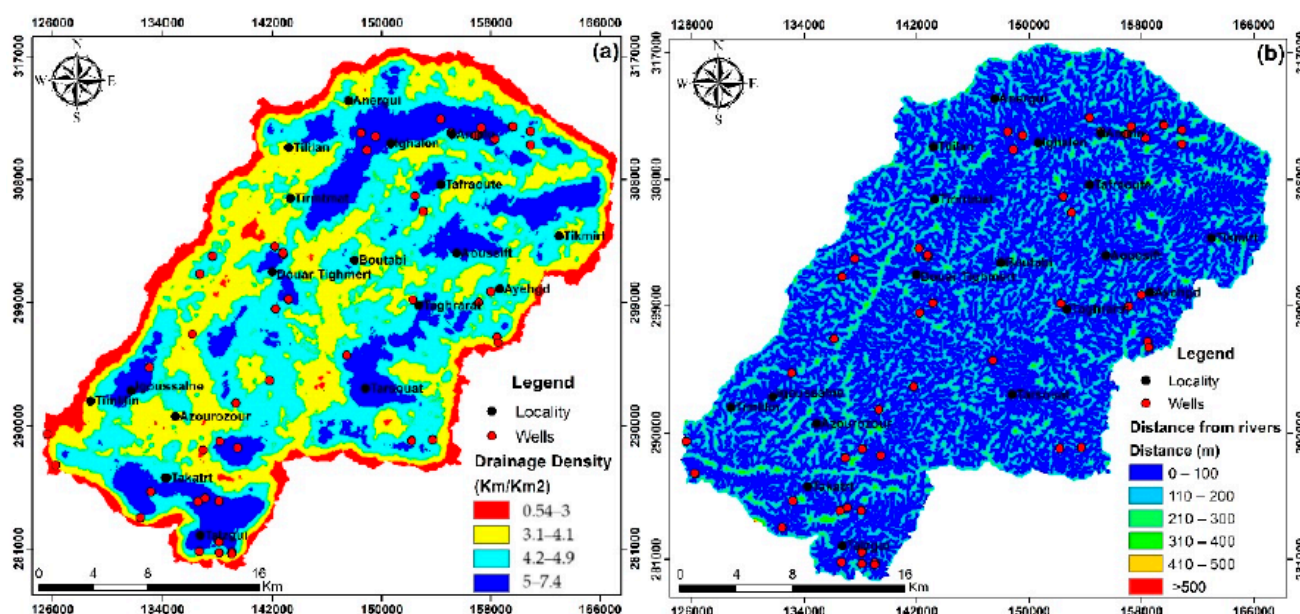
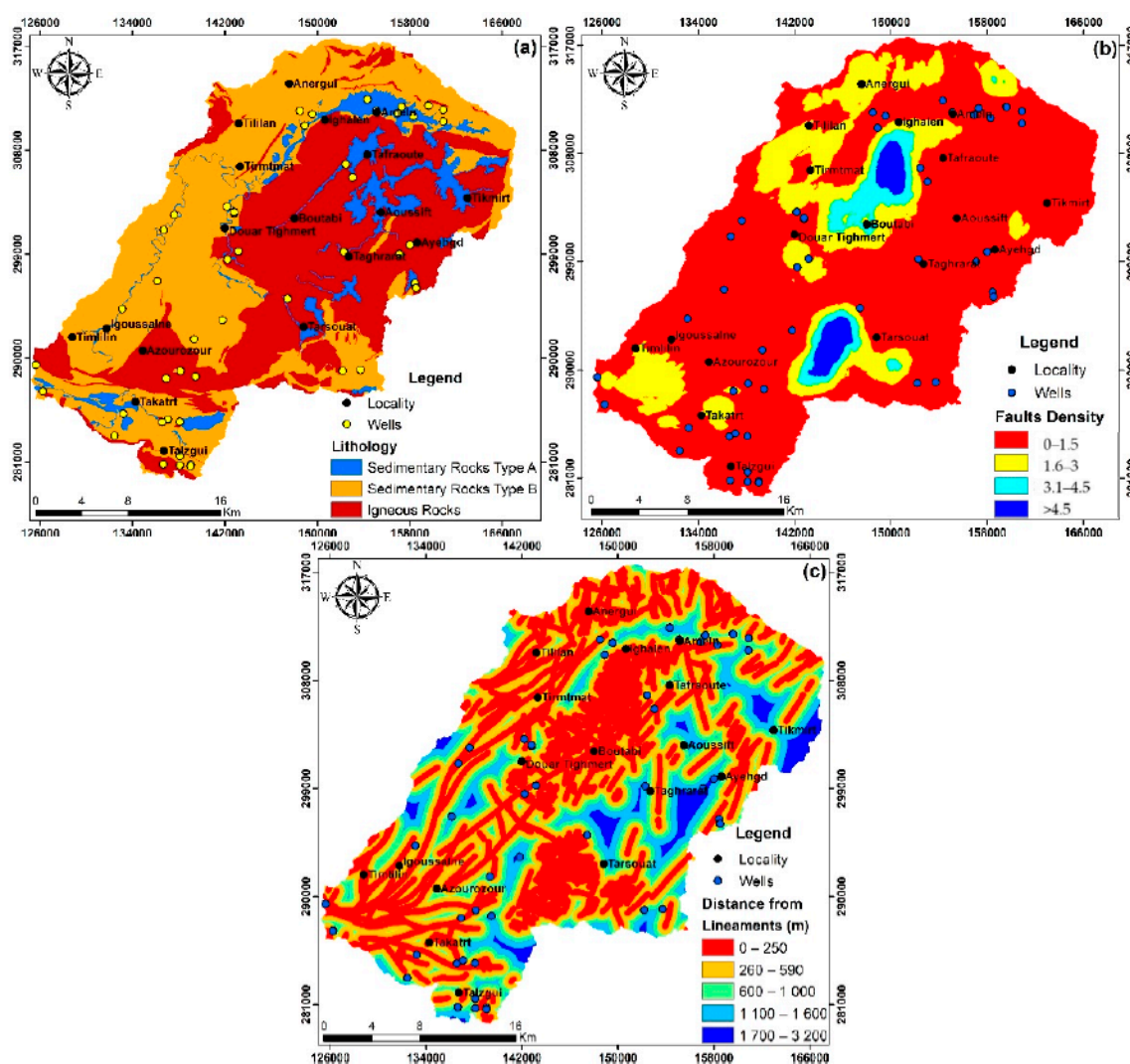


Figure 10. Hydrological factors influencing groundwater. (a) Drainage density; (b) Distance from rivers.

Based on the lithology type and geologic age of the formations, the study area was divided into 48 units. These units were classified according to their characteristics and permeabilities: sedimentary rock type (A), sedimentary rock type (B), and igneous rocks (Figure 11a). The sedimentary type (A) rocks are very permeable of the Quaternary formations, and consist of silts, screes, and pebbles, while the sedimentary type (B) rocks are moderately permeable formations of Adoudounian and Georgian ages, and consist of fractured limestones, dolomites, conglomerates, and shales. On the contrary, the sedimentary type (C) rock consists of igneous rocks that are impermeable to water filtration. The lineaments extraction shows that the NE–SW direction is the major direction detected by the 45° filter. In addition, the lineaments are dense in the north of Tafraout and in Tarçouat (Afra granites) where the geological formations are strongly tectonized and correspond to granitic arenas (Figure 11b). Furthermore, the areas close to the lineaments (300 m) are the most promising for effective infiltration; however, the effect of this parameter decreases at distances greater than 700 m (Figure 11c).



**Figure 11.** Geological factors influencing groundwater. (a) Lithology; (b) Lineaments density; (c) Distance from lineaments.

The NDVI map of the Ameln Basin reveals five interval classes varying between  $-0.12$  and  $0.38$  (Figure 12a). The high NDVI values correspond to the various valleys and topographic depressions, indicating temperate and humid areas and the increasing possibility of positive groundwater prospection. On the contrary, the NDVI negative values correspond to arid areas of low groundwater potential. On the other hand, the land surface temperature (LST) map shows values ranging from  $16$  to  $39$  °C with a mean of  $29$  °C and a standard deviation of  $3.5$  (Figure 12b). The high LST values ( $35$ – $38$  °C) correspond to the areas of low altitudes (the northern and southwestern areas of Irigh N'Tahala). The appearance of warm anomalies indicates bare land in the suburban zones. The moderate LST values ( $25$ – $32$  °C) correspond to the built-up areas in the west of Tafrout, in the north of Tarçouat, and in the southern and southeastern part of Ait Ouafqa. Due to the strong runoff in these areas, their soil is considered impermeable and indicates a low potential for groundwater. The low LST values ( $23$ – $16$  °C) correspond to the areas in the north, the south of Tizoughrane, and the central ridge of Jbel Lkest. The soil in these areas is saturated (moisture-laden), indicating moderate groundwater potential.

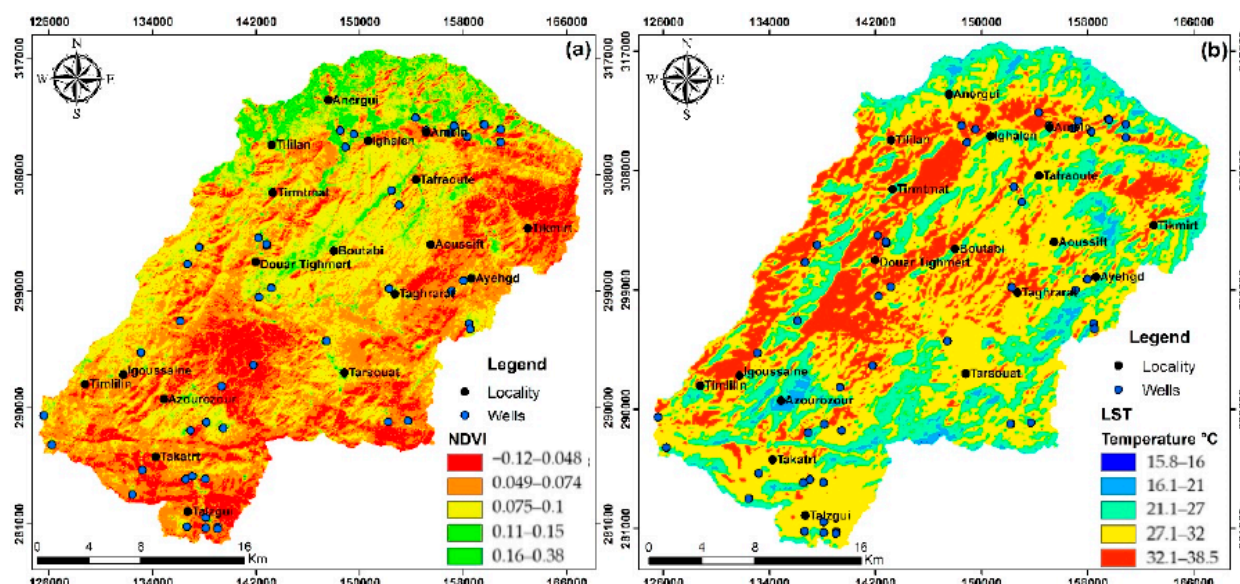


**Figure 12.** Climatological factors influencing groundwater. (a) Normalized difference vegetation index (NDVI); (b) Land surface temperature.

#### 4.2. Frequency Ratio and Shannon Entropy Result

The results of the spatial relationship between the water boreholes and conditioning factors are tabulated in Table 1. Commonly, the ratio value of 1 indicates a medium correlation; on the other hand, the ratio values greater than 1 indicate a high correlation, while the values less than 1 indicate a lower correlation e.g., [23,24,30,33]. For elevations between 800 and 1000 m, the FR had a value of 2.59, which indicates a very high probability of groundwater availability in these altitudes. Meanwhile, the elevation classes more than 1000 m had an FR value of less than 1, which indicates a low probability of groundwater availability, promoting a significant water runoff surface. In contrast, water boreholes are concentrated in areas that have a topographic wetness index (TWI) of more than 8 (FR value 2.48). In addition, the slope classes 0–5 and 5–15 showed high FR values, 2.82 and 1.13, respectively, indicating high groundwater availability. The low FR value (0.25) corresponds to the slope degree class >30. Of note is that, in this study, the FR decreases where the gradient of the slope increases. The high FR value of 7.81 corresponds to the slope length ranges of between 10–15. In terms of slope aspect, the water boreholes are dominated by slopes that have a planar aspect and orient northeast and southeast, while being less dominated by west-orienting slopes.

**Table 1.** Spatial relationship between each conditioning factor and water boreholes using the FR and SE models.

Factor	Classes	Area (Pixels)	Area (%)	Borehole No.	Borehole %	Frequency Ratio (FR)	$(E_{ij})$	$H_j$	$H_j\max$	$I_j$	$v_j$
Elevation	0–800	24,809	0.44	0	0.00	0.00	0.00	2.05	3.00	0.32	0.24
	800–1000	551,814	9.91	9	25.7	2.59	0.43				
	1000–1200	1,686,375	30.3	9	25.7	0.85	0.14				
	1200–1400	1,424,487	25.5	12	34.2	1.34	0.22				
	1400–1600	923,051	16.5	2	5.71	0.34	0.06				
	1600–1800	547,847	9.84	3	8.57	0.87	0.15				
	1800–2000	246,537	4.43	0	0.00	0.00	0.00				
Slope	>2000	160,006	2.87	0	0.00	0.00	0.00	1.42	2.00	0.29	0.33
	0–5	902,150	16.21	16	45.71	2.82	0.63				
	5–15	1,967,568	35.36	14	40.00	1.13	0.25				
	15–30	2,056,617	36.96	4	11.42	0.31	0.07				
	>30	637,524	11.45	1	2.85	0.25	0.06				

Table 1. Cont.

Factor	Classes	Area (Pixels)	Area (%)	Borehole No.	Borehole %	Frequency Ratio (FR)	( $E_{ij}$ )	$H_j$	$H_{jmax}$	$I_j$	$v_j$
Curvature	Concave	2,186,540	39.29	12	34.28	0.87	0.26	<b>1.51</b>	1.58	0.05	<b>0.05</b>
	Flat	1,077,217	19.36	11	31.42	1.62	0.49				
	Convex	2,300,102	41.34	12	34.28	0.83	0.25				
Aspect	Flat	128,012	2.30	4	11.42	4.97	0.43	<b>2.49</b>	3.32	0.25	<b>0.29</b>
	North	855,154	15.37	7	20.00	1.30	0.11				
	North east	579,523	10.41	4	11.42	1.10	0.10				
	East	2211	0.04	0	0.00	0.00	0.00				
	Southeast	759,533	13.65	6	17.14	1.26	0.11				
	South	697,033	12.52	2	5.71	0.46	0.04				
	Southwest	650,521	11.69	1	2.85	0.24	0.02				
	West	713,182	12.81	4	11.42	0.89	0.08				
	Northwest	854,813	15.36	7	20.00	1.30	0.11				
	North	323,877	5.82	0	0.00	0.00	0.00				
TWI	0–8	4,923,307	88.47	25	71.42	0.81	0.14	<b>1.45</b>	1.58	0.09	<b>0.17</b>
	8–12	511,907	9.19	8	22.85	2.48	0.43				
	>12	129,620	2.32	2	5.71	2.45	0.43				
TPI	<(−0.01)	2,492,810	44.92	15	42.85	0.95	0.27	<b>1.51</b>	1.58	0.05	<b>0.06</b>
	((−0.01)–0.01)	644,036	11.60	7	20.00	1.72	0.49				
	>0.01	2,411,692	43.46	22	37.14	0.85	0.24				
LS	0–5	5,444,001	97.82	34	97.14	0.99	0.11	<b>1.00</b>	2.00	0.75	<b>1.64</b>
	5–10	70,759	1.27	0	0.00	0.00	0.00				
	10–15	20,348	0.36	1	2.85	7.81	0.89				
	>15	29,755	0.53	0	0.00	0.00	0.00				
	0–250	2,344,136	42.123	10	28.57	0.68	0.08				
	250–500	1,229,085	22.086	10	28.57	1.29	0.15				
	500–750	764,829	13.744	6	17.14	1.25	0.15				
	750–1000	490,281	8.810	3	8.57	0.97	0.12				
	1000–1250	325,721	5.853	4	11.42	1.95	0.23				
	1250–1500	198,597	3.569	1	2.85	0.80	0.10				
Distance to Faults (m)	1500–1750	110,508	1.986	1	2.85	1.44	0.17	<b>2.73</b>	3.46	0.21	<b>0.16</b>
	1750–2000	54,126	0.973	0	0.00	0.00	0.00				
	2000–2250	26,105	0.469	0	0.00	0.00	0.00				
	2250–2500	11,242	0.202	0	0.00	0.00	0.00				
	>2500	10,296	0.185	0	0.00	0.00	0.00				
	0–1.5	4,170,521	74.94	33	94.28	1.26	0.81				
	1.5–3	1,071,774	19.26	2	5.71	0.30	0.19				
	3–4.5	203,089	3.65	0	0.00	0.00	0.00				
	>4.5	119,287	2.14	0	0.00	0.00	0.00				
	Highly permeable	517,977	9.31	11	31.42	3.38	0.69				
Lithology	Moderately permeable	2,629,577	47.25	18	51.42	1.09	0.22	<b>1.14</b>	1.58	0.28	<b>0.45</b>
	Impermeable	2,417,347	43.44	6	17.14	0.39	0.08				
	Impermeable	2,417,347	43.44	6	17.14	0.39	0.08				
Drainage Density	0–2	103,831	1.86	0	0.00	0.00	0.00	<b>1.37</b>	2.00	0.31	<b>0.30</b>
	2–4	2,085,006	37.46	6	17.14	0.46	0.12				
	4–6	3,300,306	59.30	28	80	1.35	0.35				
	>6	75,771	1.36	1	2.85	2.10	0.54				
	0–100	3,616,703	64.99	29	82.85	1.27	0.68				
Distance to Rivers (m)	100–200	1,569,527	28.20	6	17.14	0.61	0.32	<b>0.91</b>	2.58	0.65	<b>0.20</b>
	200–300	352,773	6.33	0	0.00	0.00	0.00				
	300–400	25,291	0.45	0	0.00	0.00	0.00				
	400–500	563	0.01	0	0.00	0.00	0.00				
	>500	69	0.001	0	0.00	0.00	0.00				



Table 1. Cont.

Factor	Classes	Area (Pixels)	Area (%)	Borehole No.	Borehole %	Frequency Ratio (FR)	( $E_{ij}$ )	$H_j$	$H_{jmax}$	$I_j$	$v_j$
LST (°C)	<16	21	0.002	0	0.00	0.00	0.00	<b>1.18</b>	2.32	0.49	<b>0.24</b>
	16–21	20,482	2.12	0	0.00	0.00	0.00				
	21–27	232,123	24.02	1	2.85	0.12	0.05				
	27–32	516,939	53.50	28	80	1.50	0.61				
	>32	196,534	20.34	6	17.14	0.84	0.34				
NDVI	0–0.1	873,113	90.37	27	77.14	0.85	0.25	<b>0.82</b>	1.58	0.48	<b>0.53</b>
	0.1–0.2	90,116	9.32	8	22.85	2.45	0.74				
	>0.2	2904	0.30	0	0.00	0.00	0.00				

For plan and profile curvature, the results show that the flat form had the highest FR value (1.62), while the convex form had the lowest FR value (0.83), which means that the flat and concave curvature control the groundwater availability in the study area. Furthermore, geologically, the highest values of FR (3.38) correspond to the highly permeable groups of Quaternary formations (alluvial terrace, ancient Quaternary, and scree), indicating suitable areas of water accumulation and therefore enhancing groundwater recharge. Moreover, the classes of distance from hydrographic networks 0–100 and 100–200 showed the highest FR values of 1.27 and 0.61, respectively, which means the areas corresponding to those classes and are effectively zones of the occurrence of groundwater resources. The areas of drainage density of more than 4 km/km<sup>2</sup> have higher values of FR (1.35 and 2.10), indicating soil characterized by high infiltration, which means percolation of water to the surface and then intense recharge of the aquifer, which correspond to the alluvium sediments of the Ameln Valley in the study area. In addition, the classes 250–500 m, 500–750 m, and 1000–1250 m of the distance to the lineaments have higher values of FR, 1.29, 1.25, and 1.95, respectively, which mean the areas closer to the lineaments are of importance for groundwater exploration. In our study area, the lineaments density class (0–1, 5) had an FR value of 1, 62 corresponding to the highly tectonized geological formations of Tafraout granite, Tarçouat, and the quartzite of Jbel Lkest. The topographic position index shows that flat ground surfaces (medium slope zones) have higher FR values (0.95 and 1.72), which means these areas are suitable for surface water stagnation.

The NDVI class (0.1–0.2) shows a high FR value (2.45), indicating temperate and humid areas, consequently corresponding to areas of hydrogeological potential. In addition, the higher values of FR, 0.12 and 1.20, correspond to the surface temperature class's 21–27 °C and 27–32 °C, respectively. For the Shannon entropy model, the hydrological factors, such as slope degree, slope aspect, elevation, plan curvature, profile curvature, TWI, LS, and TPI, show descendent weights 0.33, 0.29, 0.24, 0.05, 0.17, 0.24, and 0.06, respectively, which indicate that the slope degree is more suitable for hydrogeological exploration (Table 1). In addition, drainage density may be considered an important factor too, where it had a high weight value of 0.30, and also a distance from the river that shows a value weight of 0.20 (Table 1). On the other hand, lithology, lineaments, and the distance to lineaments factors have weight values of 0.45, 0.25, and 0.16, respectively, indicating that lithology and lineaments are important indicators for groundwater reservoir mapping. Similarly, the NDVI and LST correspond to high weight values (0.53 and 0.24, respectively).

Figures 13 and 14 show the FR and SE hydrogeologic potential maps, respectively, which are generated using Equations (16) and (17) based on all criteria found by the used models:

$$\begin{aligned}
 GWPI_{FR} = & [(Slopedegree_{FR}) + (Aspect_{FR}) + (Altitude_{FR}) \\
 & + (Plancurvature_{FR}) + (Profilecurvature_{FR}) + (TPI_{FR}) \\
 & + (TWI_{FR}) + (LS_{FR}) + (FaultDensity_{FR}) \\
 & + (DistancetoFaults_{FR}) + (Lithology_{FR}) \\
 & + (DrainageDensity_{FR}) + (DistancetoRivers_{FR}) \\
 & + (NDVI_{FR}) + (LST_{FR})]
 \end{aligned} \quad (16)$$

$$\begin{aligned}
 GWPI_{SE} = & [(Slopedegree_{FR} \times 0.33) + (Aspect_{FR} \times 0.29) \\
 & + (Altitude_{FR} \times 0.24) + (Plancurvature_{FR} \times 0.05) \\
 & + (Profilecurvature_{FR} \times 0.05) + (TPI_{FR} \times 0.06) \\
 & + (TWI_{FR} \times 0.17) + (LS_{FR} \times 1.64) \\
 & + (FaultDensity_{FR} \times 0.25) + (DistancetoFaults_{FR} \times 0.16) \\
 & + (Lithology_{FR} \times 0.45) + (DrainageDensity_{FR} \times 0.30) \\
 & + (DistancetoRivers_{FR} \times 0.20) + (NDVI_{FR} \times 0.53) \\
 & + (LST_{FR} \times 0.24)]
 \end{aligned} \quad (17)$$

The FR groundwater potential map reveals that the area of very low, low, moderate, high, and very high groundwater potential area covers about 12.6%, 22.7%, 32.3%, 21.7%, and 10.45% of the total study area, respectively (Figure 13, Table 2). While the SE groundwater potential map indicates that the areas of very high, high, moderate, low, and very low groundwater potential cover about 5.73%, 13.34%, 27.09%, 33.9%, and 19.84% of the total study area, respectively (Figure 14, Table 2). Consequently, the favorable areas for groundwater resources exploration are double for the FR model compared to the SE model (10.45% and 5.73% for FR and SE, respectively), while the unfavorable areas are much more for the SE model than the FR model: 19.84% and 12.6%, respectively.

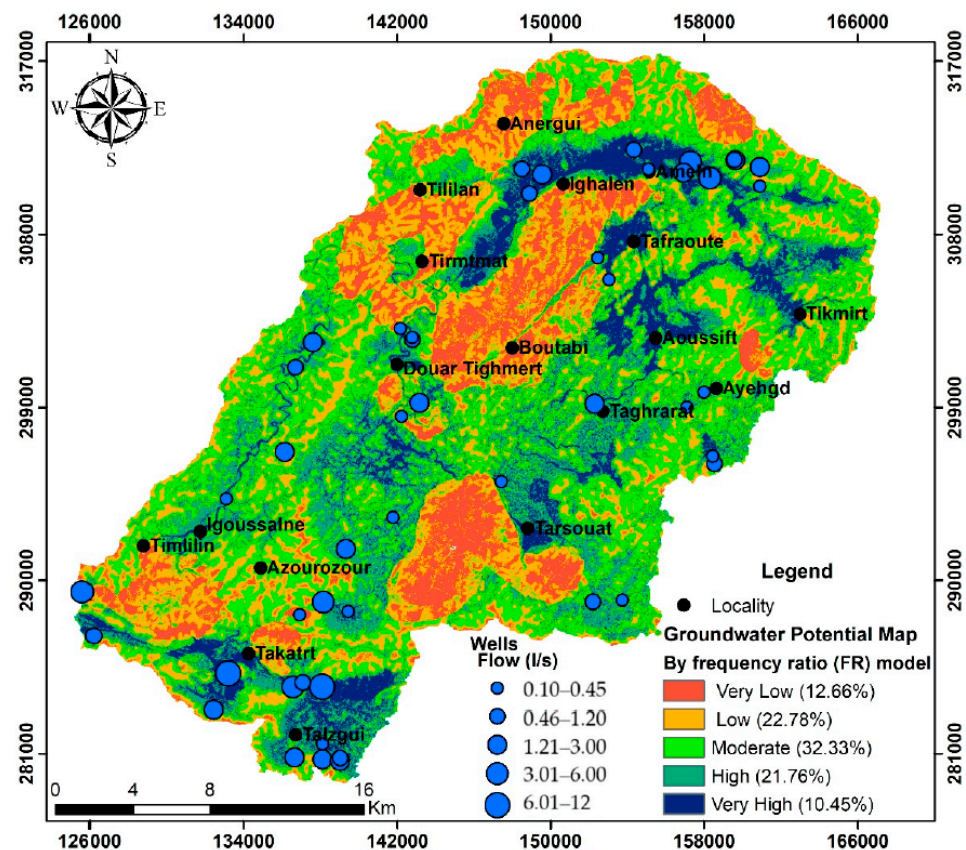


Figure 13. Groundwater potential map by the frequency ratio (FR) model.

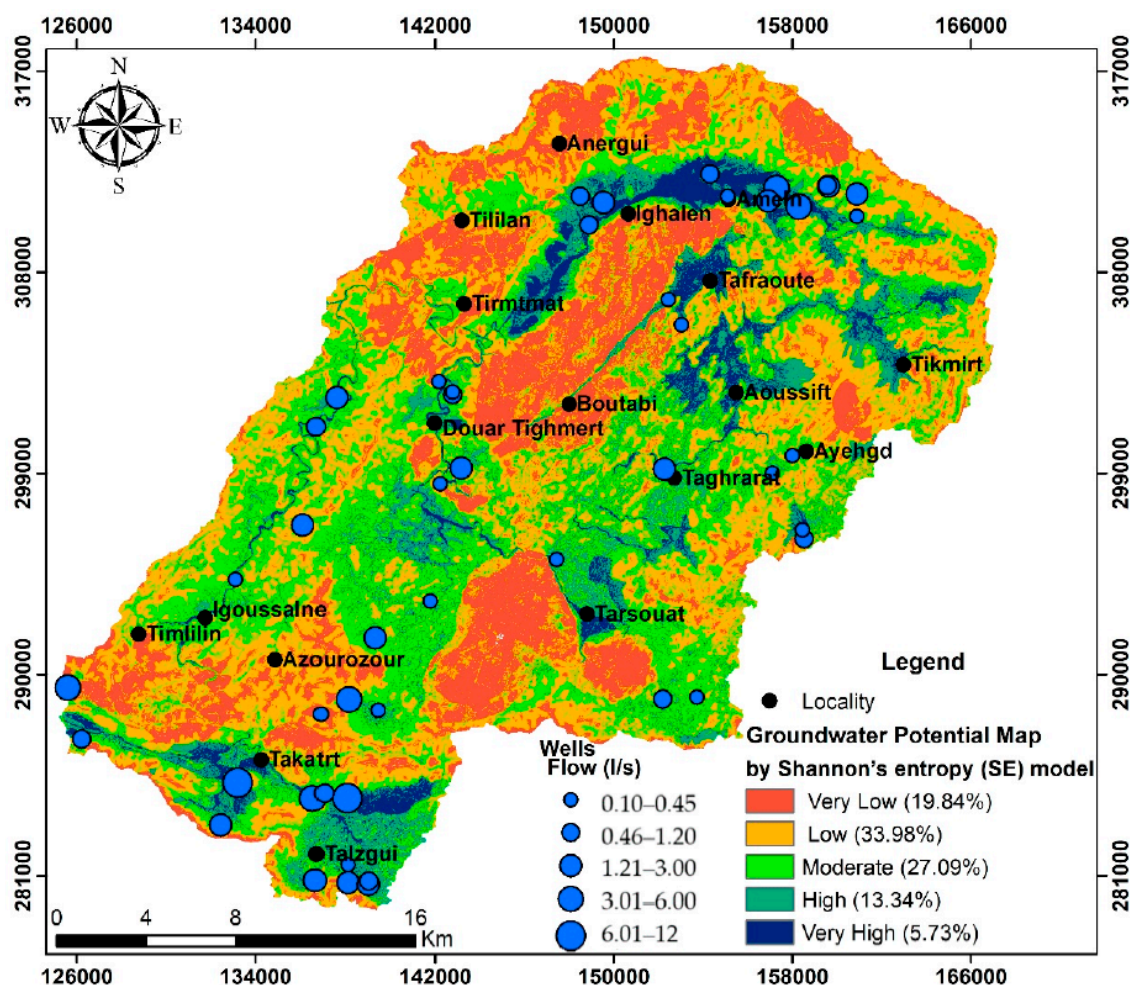


Figure 14. Groundwater potential map by Shannon's entropy (SE) model.

Table 2. Distribution of the groundwater availability classes and areas covered by each of these classes.

Groundwater Potential Zones	Frequency Ratio Model (FR)		Shannon's Entropy Model (SE)	
	Range	Area (%)	Range	Area (%)
Very Low	168–491	12.66	17.3–50.1	19.84
Low	492–643	22.78	50.2–64.8	33.98
Moderate	644–782	32.33	64.9–80.5	27.09
High	783–939	21.76	80.6–101	13.34
Very High	940–1310	10.45	102–142	5.73

In this study, the hydrogeological mapping using the frequency ratio and Shannon's entropy models highlighted the importance of using the following factors as indicators of groundwater resources availability: slope, altitudes, lithology of geological formations, lineaments (faults), and distance from them. For future water drilling in the study area, both models confirmed the suitability of several zones, such as the Ameln, Oumaghouz, and Idikel valleys that drain the northern slope of Tikmirt and the valley of Tkatrt in the south of the Ameln Basin. The aforementioned valleys are generally small alluvial deposits of the Quaternary consisting of silt, scree, and gravel. In addition, the sedimentary outcrop formations of the Adoudounian and Georgian ages, essentially consisting of fractured limestones, dolomites, conglomerates, and shale, are moderately productive. Nevertheless, the shales are generally impermeable but can be a potential hydrogeological zone for the thick altered layers forming moderate slopes in depression areas. In our study area, the shale plays the role of reservoir for the underflow of descending rivers of the Precambrian

massifs and boreholes along the valleys. In general, igneous rocks consist of rhyolites, andesites, granites, migmatites, and impermeable quartzite formations. Also, the eruptive rocks such as rhyolites, ignimbrites, and volcanic tuffs are impermeable but perhaps the groundwater potential reservoirs are found to be cracked. In our study area, all the water sources in these formations were found in fractured zones. The field survey confirms that the water sources, always of low flow, are distributed along with the contact of two different eruptive rocks (e.g., rhyolite and tuffs). In addition, these formations are marked by the presence of springs but they are always of low flow. On the other hand, at the surface of depression zones, the granites and migmatites formations are very altered, while they are not much altered in elevated areas (reliefs) where the network circulations are remarkable. In the hollows, the granites are covered by permeable arenas indicating aquifers. In other places, where the arenas are of low thickness, there are no generalized aquifers, but the alluvial aquifers that are drained by the rivers may be exploitable. Despite the slope steepness of the quartzite series of the Jbel Lkest group, it may be considered a suitable groundwater reservoir because it is very thick (more than 1000 m), is tectonized (fractured), and has fissure permeability. In addition, in the study area, the dolerites that cross the quartzites are of hydrogeological importance. In fact, at the low elevation points, the water sources were found in the quartzite–dolerite contacts forming a depression zone. In general, several springs identified in quartzites are of important flow (up to 20 L/s in the valley of Ameln at the foot of Jbel Lkest, near Tafraout city).

#### 4.3. Validation of Groundwater Potential Map

##### 4.3.1. Validation Using Wells Data

Commonly, in the context of groundwater potential map validation, the used criterion in the evaluation must reflect the reality of the field, the criterion independence principles, and the conformity of the criterion [91,92]. In this study, the visual interpretation of the overlapped water flow points (recorded from well points over the study area) on the obtained groundwater potential maps reveals that the percentage of the positive wells increases progressively toward the most productive areas (42.86% for the FR model and 30.61% for the SE model). In addition, we noted that few of these wells of low water flow are concentrated in unfavorable areas of hydrogeological importance (4.08% for the FR model and 6.12 for the SE model) (Figure 15). These findings confirm that Shannon's entropy model has a slightly better performance than the frequency ratio model in mapping groundwater potential areas.

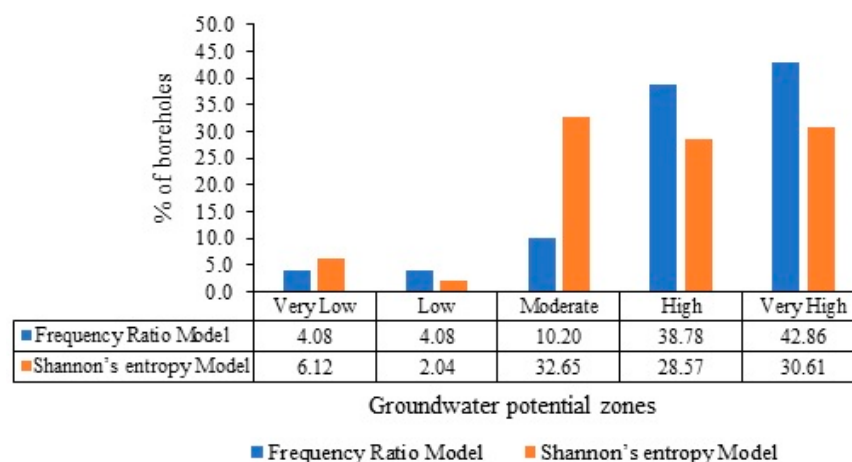


**Figure 15.** Trend histogram shows the distribution of boreholes at each class of potentialities obtained.

##### 4.3.2. Validation Using Apparent Resistivity Data

The visual interpretation of the 7200 Hz coplanar apparent resistivity map of the geological formations of about 60 m in depth indicates the presence of four areas of hydrogeological importance (Figure 16). The first one corresponds to the alluvium and



to the altered and fractured shales of the Ameln Valley, where the registered conductivity is less than 120 Ohm.m. This area is of high flow, where the water flow registered at the wells may be up to 10 L/s. On the contrary, the area in the north of the Ameln Valley shows more resistivity (>5000 Ohm.m), indicating an unfavorable area for hydrogeological exploitation. This area corresponds to the quartzite formations of Jbel Lkest, to shale-resisted alteration, or a very compact basic vein intrusion. In addition, the map shows that the second area of hydrogeological interest is located in the southwest part of Tafraout city, where a conductivity break appears. This area may correspond to a deep NE–SW fault located between two granitic bedrocks that have a resistivity of more than 5500 Ohm.m and show an average flow of 3 L/s. The third area corresponds to the Quaternary depression located in the north of Tikmirt. In this area, the apparent resistivity of the sediments covering resistant conglomerate of about 60 m of thickness is less than 100 Ohm.m. Further, due to the major and deep fault of Tighmi-Tizi Oumanouz oriented E–W (the southern equivalent of the Ameln fault), and due to the intense alteration of fractured shales, the geological formations located in the south of the Ameln Basin show a resistivity of less than 150 Ohm.m, indicating an area of hydrogeological potential that is favorable for exploitation. This was confirmed by the flow rate of the aquifer productivity, which can reach 12 L/s. Overall, these findings highlight the importance of using the apparent resistivity data to confirm the developed hydrogeological maps of both models. Of note is that the areas of high conductivity indicate potential drinking water targets.

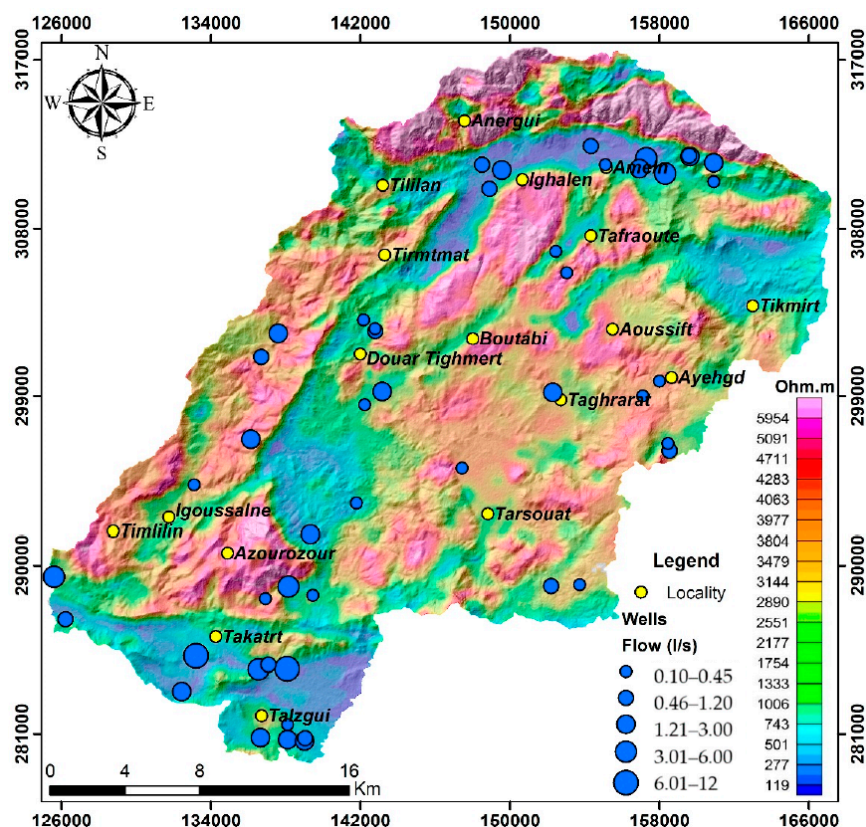


**Figure 16.** The 7200 Hz apparent resistivity map of the Ameln Basin shows the different areas of hydrogeological importance.

## 5. Conclusions

In Morocco, for many years, the Water Basin Agencies, responsible for water resources planning, management, and protection, tried to find an adequate approach to identify the most favorable zones for water exploitation to serve the population needs, especially in rural areas. The present study represents an approach anticipated to map groundwater potential areas in a fractured semi-arid area (Ameln Basin, Morocco). In this study, two

groundwater potential area maps were prepared using the FR and SE models based on the geologic, topographic, hydrologic, and climatic data of the study area. The obtained maps were verified with wells and apparent resistivity data. The SE model reveals slope length, lithology, and slope degree that control the availability of groundwater in the study area more than the other factors. In contrast, for the FR model, the controlling factors are slope aspect, altitude, curvatures, and distance from lineament networks. In general, both models show promising results in terms of identification of favorable areas for groundwater exploration, with a preference for the FR model that shows more percentage of surface area than the SE model (10.45% and 5.73% of the total study area for FR and SE, respectively). The favorable areas correspond to the Ameln and Oumaghouz valleys, altered surface depressions in the north of Tafraout, and the Quaternary formations located in the south of Tarçouat, in the north of Aoussift and Tikmirt, and in the southern part of the Ameln Basin. In addition, 42.86% and 30.61% of the total surface area are concordant to the positive wells (high water flow) for the FR and SE models, respectively, indicating a slightly better performance of the FR model in mapping groundwater potential areas than the SE model. Eventually, despite the limited number of wells in our study area used in the verification step, the obtained results allow us to conclude that both methods may be considered suitable tools for facilitating and orienting hydrogeological exploration strategies (water resources management, development, and exploitation). The conclusion is that both models can produce groundwater prospecting areas with very good accuracy. Future work should highlight the integration of mathematical approaches such as the boosted regression tree or advanced machine learning. The efficacy of the remote sensing methodology in groundwater delineation could be further improved by considering a sufficient quantity of information and data that have direct or indirect control over groundwater storage and occurrence. Indeed, to better appreciate the accuracy of these methods and to improve them, specific surveys are required in the most reliable and productive areas. In addition, the integration of aeromagnetic, gravimetric, and radar data will be helpful to enhance the lineaments map and then improve the accuracy of the used methods.

**Author Contributions:** Conceptualization, K.B. and F.A.; methodology, K.B., F.A., A.A., A.T., M.Y., and B.P.; software, K.B. and A.A.; validation, M.Y., B.P. and M.A.; formal analysis, K.B., F.A., A.A. and A.T.; investigation, K.B.; resources, K.B.; data curation, K.B.; writing—original draft preparation, K.B., F.A., A.A., A.T., M.Y., B.P., K.A., M.S.F. and M.A.; writing—review and editing, M.Y., B.P. and M.A.; visualization, K.B.; supervision, F.A.; project administration, M.A.; funding acquisition, K.A. and M.S.F. All authors have read and agreed to the published version of the manuscript.

**Funding:** This research was funded by Researchers Supporting Project number (RSP-2021/351), King Saud University, Riyadh, Saudi Arabia.

**Institutional Review Board Statement:** Not applicable.

**Informed Consent Statement:** Not applicable.

**Data Availability Statement:** The data presented in this study are available on request from the corresponding authors.

**Conflicts of Interest:** The authors declare no conflict of interest.

## References

1. Bouchaou, L.; Tagma, T.; Boutaleb, S.; Hssaisoune, M.; El Morjani, Z.E.A. Climate change and its impacts on groundwater resources in Morocco: The case of the Souss-Massa Basin. In *Climate Change Effects on Groundwater Resources. A Global Synthesis of Findings and Recommendations*; Treidel, H., Martin-Bordes, J.L., Gurdak, J.J., Eds.; UNESCO, International Hydrological Programme: Paris, France, 2011; pp. 129–143.
2. Seif-Ennasr, M.; Zaaboul, R.; Hirich, A.; Caroletti, G.N.; Bouchaou, L.; Morjani, Z.E.A.E.; Beraaouz, E.H.; McDonnell, R.A.; Choukr-Allah, R. Climate change and adaptive water management measures in Chtouka Aït Baha region (Morocco). *Sci. Total Environ.* **2016**, *573*, 862–875. [[CrossRef](#)] [[PubMed](#)]

3. Bouchaou, L.; Hirich, A.; Choukr-Allah, R.; Bouaakaz, B.; Malki, M.; Abahous, H.; Nrhira, A. Climate change and water valuation in Souss-Massa region: Management and adaptive measures. In Proceedings of the 10th World Congress of EWRA on Water Resources and Environment, Athens, Greece, 5–9 July 2017; Rhei, P., Tsakiris, G., Tsihrintzis, V.A., Vangelis, H., Tigkas, D., Eds.; EWRA: Catania, Italy, 2017; pp. 835–843.
4. Seif-Ennasr, M.; Hirich, A.; El Morjani, Z.E.A.; Choukr-Allah, R.; Zaaboul, R.; Nrhira, A.; Malki, M.; Bouchaou, L.; Beraaouz, E.H. Assessment of Global Change Impacts on Groundwater Resources in Souss-Massa Basin. In *Water Resources in Arid Areas: The Way Forward*; Abdalla, O., Kacimov, A., Chen, M., Al-Maktoumi, A., Al-Hosni, T., Clark, I., Eds.; Springer: Berlin/Heidelberg, Germany, 2017; pp. 115–140.
5. Kadi, M.A.; Ziyad, A. Integrated Water Resources Management in Morocco. In *Global Water Security*; World Water Council, Ed.; Springer: Singapore, 2018; pp. 143–163.
6. Benjmel, K.; Amraoui, F.; Boutaleb, S.; Ouchchen, M.; Tahiri, A.; Touab, A. Mapping of Groundwater Potential Zones in Crystalline Terrain Using Remote Sensing, GIS Techniques, and Multicriteria Data Analysis (Case of the Ighrem Region, Western Anti-Atlas, Morocco). *Water* **2020**, *12*, 471. [\[CrossRef\]](#)
7. Hssaisoune, M.; Bouchaou, L.; Sifeddine, A.; Bouimetarhan, I.; Chehbouni, A. Moroccan Groundwater Resources and Evolution with Global Climate Changes. *Geosciences* **2020**, *10*, 81. [\[CrossRef\]](#)
8. Yousif, M. A new theory to enhance the groundwater-related decisions based on deciphering the palaeohydrologic regime under climate change in the Sahara. *Model. Earth Syst. Environ.* **2021**, 1–11. [\[CrossRef\]](#)
9. Salama, D.S.; Yousif, M.; Gedamy, Y.; Ahmed, H.M.; Ali, M.E.; Shoukry, E.M. Satellite observations for monitoring atmospheric NO<sub>2</sub> in correlation with the existing pollution sources under arid environment. *Model. Earth Syst. Environ.* **2022**, 1–19. [\[CrossRef\]](#)
10. Hsissou, Y.; Mudry, J.; Bouchaou, L.; Chauve, P.; Mania, J. Use of chemical tracy to study acquisition modality of mineralization and behaviour of unconfined groundwater under semi-arid climate: The case study of the Souss plain (Morocco). *Environ. Geol.* **2002**, *42*, 672–680.
11. Ahkhouk, S.; Hsissou, Y.; Bouchaou, L.; Krimissa, M.; Mania, J. Impact des fertilisants agricoles et du mode d'irrigation sur la qualité des eaux souterraines (cas de la nappe libre des Chtouka, bassin du Souss–Massa, Maroc). *Afr. Geosci. Rev.* **2003**, *10*, 355–364.
12. Bouchaou, L.; Michelot, J.; Vengosh, A.; Hsissou, Y.; Qurtobi, M.; Gaye, C.; Bullen, T.; Zuppi, G. Application of multiple isotopic and geochemical tracers for investigation of recharge, salinization, and residence time of water in the Souss–Massa aquifer, southwest of Morocco. *J. Hydrol.* **2008**, *352*, 267–287. [\[CrossRef\]](#)
13. Tagma, T.; Hsissou, Y.; Bouchaou, L.; Bouragba, L.; Boutaleb, S. Groundwater nitrate pollution in Souss-Massa Basin (south–west Morocco). *Afr. J. Environ. Sci. Technol.* **2009**, *3*, 301–309.
14. Danni, S.O.; Bouchaou, L.; Elmouden, A.; N'Da, B.; Brahim, Y.A.; Malki, M. Isotopic and Chemical Tracers for the Sustainable Management of Water Resources in Semi-arid Area: Case of Massa Catchment, Morocco. In *Groundwater and Global Change in the Western Mediterranean Area*; Calvache, M., Duque, C., Pulido-Velazquez, D., Eds.; Springer: Cham, Germany, 2018; pp. 261–268.
15. Shekhar, S.; Pandey, A.C. Delineation of groundwater potential zone in hard rock terrain of India using remote sensing, geographical information system (GIS) and analytic hierarchy process (AHP) techniques. *Geocarto Int.* **2014**, *30*, 402–421. [\[CrossRef\]](#)
16. Ghosh, D.; Mandal, M.; Banerjee, M.; Karmakar, M. Impact of hydro-geological environment on availability of groundwater using analytical hierarchy process (AHP) and geospatial techniques: A study from the upper Kangsabati river basin. *Groundw. Sustain. Dev.* **2020**, *11*, 100419. [\[CrossRef\]](#)
17. Mukherjee, I.; Singh, U. Delineation of groundwater potential zones in a drought-prone semi-arid region of east India using GIS and analytical hierarchical process techniques. *CATENA* **2020**, *194*, 104681. [\[CrossRef\]](#)
18. Le Page, M.; Berjamy, B.; Fakir, Y.; Bourgin, F.; Jarlan, L.; Abourida, A.; Benrhanem, M.; Jacob, G.; Huber, M.; Sghrer, F.; et al. An Integrated DSS for Groundwater Management Based on Remote Sensing. The Case of a Semi-arid Aquifer in Morocco. *Water Resour. Manag.* **2012**, *26*, 3209–3230. [\[CrossRef\]](#)
19. Goitsemang, T.; Das, D.M.; Raul, S.K.; Subudhi, C.R.; Panigrahi, B. Assessment of Groundwater Potential in the Kalahandi District of Odisha (India) Using Remote Sensing, Geographic Information System and Analytical Hierarchy Process. *J. Indian Soc. Remote Sens.* **2020**, *48*, 1739–1753. [\[CrossRef\]](#)
20. Allafta, H.; Opp, C.; Patra, S. Identification of Groundwater Potential Zones Using Remote Sensing and GIS Techniques: A Case Study of the Shatt Al-Arab Basin. *Remote Sens.* **2020**, *13*, 112. [\[CrossRef\]](#)
21. Achu, A.L.; Thomas, J.; Reghunath, R. Multi-criteria decision analysis for delineation of groundwater potential zones in a tropical river basin using remote sensing, GIS and analytical hierarchy process (AHP). *Groundw. Sustain. Dev.* **2020**, *10*, 100365. [\[CrossRef\]](#)
22. Qadir, J.; Bhat, M.S.; Alam, A.; Rashid, I. Mapping groundwater potential zones using remote sensing and GIS approach in Jammu Himalaya, Jammu and Kashmir. *GeoJournal* **2019**, *85*, 487–504. [\[CrossRef\]](#)
23. Shao, Z.; Huq, E.; Cai, B.; Altan, O.; Li, Y. Integrated remote sensing and GIS approach using Fuzzy-AHP to delineate and identify groundwater potential zones in semi-arid Shanxi Province, China. *Environ. Model. Softw.* **2020**, *134*, 104868. [\[CrossRef\]](#)
24. Todd, D.K.; Mays, L.W. *Groundwater Hydrology*, 3rd ed.; Wiley: Hoboken, NJ, USA, 2004.
25. Jha, M.K.; Chowdary, V.M.; Chowdhury, A. Groundwater assessment in Salboni Block, West Bengal (India) using remote sensing, geographical information system and multi-criteria decision analysis techniques. *Hydrogeol. J.* **2010**, *18*, 1713–1728. [\[CrossRef\]](#)



26. Goodchild, M.F. Geographic information systems. In *Encyclopedia of Theoretical Ecology*; University of California Press: Oakland, CA, USA, 2012; pp. 341–345.
27. Machiwal, D.; Jha, M.K.; Mal, B.C. Assessment of Groundwater Potential in a Semi-Arid Region of India Using Remote Sensing, GIS and MCDM Techniques. *Water Resour. Manag.* **2010**, *25*, 1359–1386. [\[CrossRef\]](#)
28. Das, N.; Mukhopadhyay, S. Application of multi-criteria decision making technique for the assessment of groundwater potential zones: A study on Birbhum district, West Bengal, India. *Environ. Dev. Sustain.* **2018**, *22*, 931–955. [\[CrossRef\]](#)
29. Lee, S.; Hyun, Y.; Lee, M.-J. Groundwater Potential Mapping Using Data Mining Models of Big Data Analysis in Goyang-si, South Korea. *Sustainability* **2019**, *11*, 1678. [\[CrossRef\]](#)
30. Aouragh, M.H.; Essahlaoui, A.; El Ouali, A.; El Hmaidi, A.; Kamel, S. Groundwater potential of Middle Atlas plateaus, Morocco, using fuzzy logic approach, GIS and remote sensing. *Geomat. Nat. Hazards Risk* **2016**, *8*, 194–206. [\[CrossRef\]](#)
31. Kazakis, N. Delineation of Suitable Zones for the Application of Managed Aquifer Recharge (MAR) in Coastal Aquifers Using Quantitative Parameters and the Analytical Hierarchy Process. *Water* **2018**, *10*, 804. [\[CrossRef\]](#)
32. Nouayti, A.; Khattach, D.; Hilali, M.; Nouayti, N. Mapping potential areas for groundwater storage in the High Guir Basin (Morocco): Contribution of remote sensing and geographic information system. *J. Groundw. Sci. Eng.* **2019**, *7*, 309–322.
33. Agarwal, E.; Agarwal, R.; Garg, R.D.; Garg, P.K. Delineation of groundwater potential zone: An AHP/ANP approach. *J. Earth Syst. Sci.* **2013**, *122*, 887–898. [\[CrossRef\]](#)
34. Siddi Raju, R.; Sudarsana Raju, G.; Ravikumar, M.; Raghubabu, K. Applications of remote sensing and GIS, for identification of groundwater prospecting zones in and Around Nandalur, YSR District. *IJEP* **2016**, *36*, 293–304.
35. Das, S.; Gupta, A.; Ghosh, S. Exploring groundwater potential zones using MIF technique in semi-arid region: A case study of Hingoli district, Maharashtra. *Spat. Inf. Res.* **2017**, *25*, 749–756. [\[CrossRef\]](#)
36. Naghibi, S.A.; Pourghasemi, H.R.; Dixon, B. GIS-based groundwater spring potential using boosted regression tree, classification and regression tree, and random forest machine learning models in Iran. *Environ. Monit. Assess.* **2016**, *188*, 44. [\[CrossRef\]](#)
37. Maskooni, E.K.; Naghibi, S.; Hashemi, H.; Berndtsson, R. Application of Advanced Machine Learning Algorithms to Assess Groundwater Potential Using Remote Sensing-Derived Data. *Remote Sens.* **2020**, *12*, 2742. [\[CrossRef\]](#)
38. Chaudhari, R.V.; Dhanesh, L.; Sayantan, D.; Bhavna, U.; Saheb, H. Weighted overlay analysis for delineation of groundwater potential zone: A case study of pirangut river basin. *Int. J. Remote Sens. Geosci.* **2018**, *7*, 2319–3484.
39. Ozdemir, A. Using a binary logistic regression method and GIS for evaluating and mapping the groundwater spring potential in the Sultan Mountains (Aksehir, Turkey). *J. Hydrol.* **2011**, *405*, 123–136. [\[CrossRef\]](#)
40. Razavi-Termeh, S.V.; Sadeghi-Niaraki, A.; Choi, S.-M. Groundwater Potential Mapping Using an Integrated Ensemble of Three Bivariate Statistical Models with Random Forest and Logistic Model Tree Models. *Water* **2019**, *11*, 1596. [\[CrossRef\]](#)
41. Naghibi, S.A.; Pourghasemi, H.R.; Pourtaghi, Z.S.; Rezaei, A. Groundwater qanat potential mapping using frequency ratio and Shannon's entropy models in the Moghan watershed, Iran. *Earth Sci. Inform.* **2014**, *8*, 171–186. [\[CrossRef\]](#)
42. Elvis, B.W.W.; Arsène, M.; Théophile, N.M.; Bruno, K.M.E.; Olivier, O.A. Integration of shannon entropy (SE), frequency ratio (FR) and analytical hierarchy process (AHP) in GIS for suitable groundwater potential zones targeting in the Yoyo river basin, Méiganga area, Adamawa Cameroon. *J. Hydrol. Reg. Stud.* **2022**, *39*, 100997. [\[CrossRef\]](#)
43. Bednarik, M.; Magulová, B.; Matys, M.; Marschalko, M. Landslide susceptibility assessment of the Kralovany–Liptovský Mikuláš railway case study. *Phys. Chem. Earth* **2010**, *35*, 162–171. [\[CrossRef\]](#)
44. Al-Abadi, A.M.; Al-Temmeme, A.A.; Al-Ghanimy, M.A. A GIS-based combining of frequency ratio and index of entropy approaches for mapping groundwater availability zones at Badra–Al Al-Gharbi–Teeb areas, Iraq. *Sustain. Water Resour. Manag.* **2016**, *2*, 265–283. [\[CrossRef\]](#)
45. Najine, A.; Jaffal, M.; El Khammari, K.; Aifa, T.; Kattach, D.; Himi, M.; Casas, A.; Badrane, S.; Aqil, H. Contribution de la gravimétrie à l'étude de la structure du bassin de Tadla (Maroc): Implications hydrogéologiques. *Comptes Rendus Geosci.* **2006**, *338*, 676–682. [\[CrossRef\]](#)
46. Bouchaou, L.; Boutaleb, S.; Boualoul, M.; Oudra, M. Application of remote-sensing and surface geophysics for groundwater prospecting in a hard rock terrain, Morocco. In *Applied Groundwater Studies in Africa*; Adelana, S.M.A., MacDonald, A.M., Eds.; IAH Book Series; CRC Press: Boca Raton, FL, USA; Balkema: Leiden, The Netherlands, 2008; pp. 215–227.
47. Rochdane, S.; El Mandour, A.; Jaffal, M.; Himi, M.; Casas, A.; Amrhar, M.; Karroum, M. Géométrie de l'aquifère du Haouz oriental et Tassaout amont, Maroc occidental: Approche géophysique et hydrogéologique. *Hydrol. Sci. J.* **2015**, *60*, 133–144. [\[CrossRef\]](#)
48. Elmahdy, S.I.; Mohamed, M.M. Probabilistic frequency ratio model for groundwater potential mapping in Al Jaww plain, UAE. *Arab. J. Geosci.* **2014**, *8*, 2405–2416. [\[CrossRef\]](#)
49. Moghaddam, D.D.; Rezaei, M.; Pourghasemi, H.R.; Pourtaghie, Z.S.; Pradhan, B. Groundwater spring potential mapping using bivariate statistical model and GIS in the Taleghan Watershed, Iran. *Arab. J. Geosci.* **2013**, *8*, 913–929. [\[CrossRef\]](#)
50. Leblanc, M. Ophiolites précambriennes et gîtes arséniés de cobalt (Bou-Azzer, Maroc). *Notes Mém. Serv. Géol. Maroc.* **1975**, *280*, 306p.
51. Charlot, R. The Precambrian of the Anti-Atlas (Morocco): A geochronological synthesis. *Precambrian Res.* **1976**, *3*, 273–299. [\[CrossRef\]](#)
52. Charlot, R. Caractérisation des Événements Éburnéens et Pan-Africains dans l'Anti-Atlas Marocain. Apport de la Méthode Géochronologique Rb/Sr. Ph.D. Thesis, Université de Rennes, Rennes, France, 1978.



53. Hassenforder, B. La Tectonique Panafricaine et Varisque de l'Anti-Atlas dans le Massif du Kerdous (Maroc). Ph.D. Thesis, Université de Strasbourg, Strasbourg, France, 1987.
54. Saquaque, A.; Admou, H.; Cisse, A.; Benyoussef, A.; Reuber, I. Les intrusions calco—Alcalines de la boutonnière de Bou-Azzer-El Graâra (Anti-Atlas): Marqueurs de la déformation panafricaine majeure dans un contexte de collision d'arc. *CR Acad. Sci.* **1989**, *308*, 1279–1283.
55. Thomas, R.; Chevallier, L.; Gresse, P.; Harmer, R.; Eglington, B.; Armstrong, R.; de Beer, C.; Martini, J.; de Kock, G.; Macey, P.; et al. Precambrian evolution of the Sirwa Window, Anti-Atlas Orogen, Morocco. *Precambrian Res.* **2002**, *118*, 1–57. [\[CrossRef\]](#)
56. Gasquet, D.; Chevremont, P.; Baudin, T.; Chalot-Prat, F.; Guerrot, C.; Cocherie, A.; Roger, J.; Hassenforder, B.; Cheilletz, A. Polycyclic magmatism in the Tagragra d'Akka and Kerdous-Tafeltast inliers (Western Anti-Atlas, Morocco). *J. Afr. Earth Sci.* **2004**, *39*, 267–275. [\[CrossRef\]](#)
57. Thomas, R.; Fekkak, A.; Ennih, N.; Errami, E.; Loughlin, S.; Gresse, P.; Chevallier, L.; Liegeois, J.-P. A new lithostratigraphic framework for the Anti-Atlas Orogen, Morocco. *J. Afr. Earth Sci.* **2004**, *39*, 217–226. [\[CrossRef\]](#)
58. Benziane, F. Lithostratigraphie et Évolution Géodynamique de l'Anti-Atlas (Maroc) du Paléoprotérozoïque au Néoprotérozoïque: Exemples de la Boutonnière de Tagragra de Tata et du Jbel Saghro. Ph.D. Thesis, Université de Savoie, Chambéry, France, 2007.
59. Ennih, N.; Liegeois, J.-P. The boundaries of the West African craton, with special reference to the basement of the Moroccan metacratonic Anti-Atlas belt. *Geol. Soc. Lond. Spec. Publ.* **2008**, *297*, 1–17. [\[CrossRef\]](#)
60. Gasquet, D.; Ennih, N.; Liégeois, J.P.; Soulaïmani, A.; Michard, A. The Pan-African belt. In *Continental Evolution: The Geology of Morocco*; Michard, A., Saddiqi, O., Chalouan, A., Frizon de Lamotte, D., Eds.; Springer: Berlin/Heidelberg, Germany, 2008; Volume 116, pp. 33–64.
61. Soulaïmani, A.; Ouanaïmi, H.; Saddiqi, O.; Baïdier, L.; Michard, A. The Anti-Atlas Pan-African Belt (Morocco): Overview and pending questions. *Comptes Rendus Geosci.* **2018**, *350*, 279–288. [\[CrossRef\]](#)
62. Hassenforder, B. Evolution tectono-métamorphique du socle du Kerdous (Anti-Atlas occidental, Maroc) dans le cadre des orogénèses éburnéenne et pan-africaine. *Sci. Géol. Bull.* **1978**, *31*, 21–31. [\[CrossRef\]](#)
63. Hassenforder, B. Les mylonites de la zone de faille ductile pan-africaine des Ameln (Kerdous, Anti-Atlas occidental, Maroc). Une analyse pétrostructurale de la déformation. *Sci. Géol. Bull.* **1985**, *38*, 215–226.
64. Nachit, H.; Barbey, P.; Pons, J.; Burg, J.P. L'Eburnéen existe-t-il dans l'Anti-Atlas marocain? L'exemple du massif du Kerdous. *CR Acad. Sci.* **1996**, *322*, 677–683.
65. Soulaïmani, A.; Essaïfi, A.; Youbi, N.; Hafid, A. Les marqueurs structuraux et magmatiques de l'extension crustale au Protérozoïque terminal-Cambrien basal autour du massif de Kerdous (Anti-Atlas occidental, Maroc). *Comptes Rendus Geosci.* **2004**, *336*, 1433–1441. [\[CrossRef\]](#)
66. Barbey, P.; Nachit, H.; Pons, J. Magma-host interactions during differentiation and emplacement of a shallow-level, zoned granitic pluton (Tarçouate pluton, Morocco): Implications for magma emplacement. *Lithos* **2001**, *58*, 125–143. [\[CrossRef\]](#)
67. Benssaou, M.; Hamoumi, N. The western Anti-Atlas of Morocco: Sedimentological and palaeogeographical formation studies in the Early Cambrian. *J. Afr. Earth Sci.* **2001**, *32*, 351–372. [\[CrossRef\]](#)
68. Razandi, Y.; Pourghasemi, H.R.; Neisani, N.S.; Rahmati, O. Application of analytical hierarchy process, frequency ratio, and certainty factor models for groundwater potential mapping using GIS. *Earth Sci. Inform.* **2015**, *8*, 867–883. [\[CrossRef\]](#)
69. Mogaji, K.A.; Lim, H.S.; Abdullah, K. Regional prediction of groundwater potential mapping in a multifaceted geology terrain using GIS-based Dempster-Shafer model. *Arab. J. Geosci.* **2014**, *8*, 3235–3258. [\[CrossRef\]](#)
70. Burrough, P.A.; McDonnell, R.A. *Principle of Geographic Information Systems*; Oxford University Press: Oxford, UK, 1998.
71. Ercanoglu, M.; Gokceoglu, C. Assessment of landslide susceptibility for a landslide-prone area (north of Yenice, NW Turkey) by fuzzy approach. *Env. Geol.* **2002**, *41*, 720–730.
72. Aniya, M. Landslide-susceptibility mapping in the Anahata river basin, Japan. *Ann. Assoc. Am. Geogr.* **1985**, *75*, 102–114. [\[CrossRef\]](#)
73. Manap, M.A.; Nampak, H.; Pradhan, B.; Lee, S.; Sulaiman, W.N.A.; Ramli, M.F. Application of probabilistic-based frequency ratio model in groundwater potential mapping using remote sensing data and GIS. *Arab. J. Geosci.* **2012**, *7*, 711–724. [\[CrossRef\]](#)
74. Moore, I.D.; Grayson, R.B.; Ladson, A.R. Digital terrain modelling: A review of hydrological, geomorphological, and biological applications. *Hydrol. Process.* **1991**, *5*, 3–30. [\[CrossRef\]](#)
75. Wischmeier, W.H.; Smith, D.D. *Predicting Rainfall Erosion Losses—A Guide to Conservation Planning*; U.S. Department of Agriculture, Science and Education Administration: Hyattsville, MD, USA, 1978.
76. Moore, I.D.; Burch, G.J. Sediment Transport Capacity of Sheet and Rill Flow: Application of Unit Stream Power Theory. *Water Resour. Res.* **1986**, *22*, 1350–1360. [\[CrossRef\]](#)
77. De Reu, J.; Bourgeois, J.; Bats, M.; Zwertvaegher, A.; Gelorini, V.; De Smedt, P.; Chu, W.; Antrop, M.; De Maeyer, P.; Finke, P.; et al. Application of the topographic position index to heterogeneous landscapes. *Geomorphology* **2013**, *186*, 39–49. [\[CrossRef\]](#)
78. Magesh, N.S.; Chandrasekar, N.; Soundranayagam, J.P. Delineation of groundwater potential zones in Theni district, Tamil Nadu, using remote sensing, GIS and MIF techniques. *Geosci. Front.* **2012**, *3*, 189–196. [\[CrossRef\]](#)
79. Chowdhury, A.; Jha, M.K.; Chowdary, V.M. Delineation of groundwater recharge zones and identification of artificial recharge sites in West Medinipur district, West Bengal, using RS, GIS and MCDM techniques. *Environ. Earth Sci.* **2010**, *59*, 1209–1222. [\[CrossRef\]](#)

80. Gannouni, S.; Gabtni, H. Structural Interpretation of Lineaments by Satellite Image Processing (Landsat TM) in the Region of Zahret Medien (Northern Tunisia). *J. Geogr. Inf. Syst.* **2015**, *07*, 119–127. [[CrossRef](#)]
81. Mandal, U.; Sahoo, S.; Munusamy, S.B.; Dhar, A.; Panda, S.N.; Kar, A.; Mishra, P.K. Delineation of Groundwater Potential Zones of Coastal Groundwater Basin Using Multi-Criteria Decision Making Technique. *Water Resour. Manag.* **2016**, *30*, 4293–4310. [[CrossRef](#)]
82. Chen, W.; Li, H.; Hou, E.; Wang, S.; Wang, G.; Panahi, M.; Li, T.; Peng, T.; Guo, C.; Niu, C.; et al. GIS-based groundwater potential analysis using novel ensemble weights-of-evidence with logistic regression and functional tree models. *Sci. Total Environ.* **2018**, *634*, 853–867. [[CrossRef](#)]
83. Miraki, S.; Zanganeh, S.H.; Chapi, K.; Singh, V.P.; Shirzadi, A.; Shahabi, H.; Pham, B.T. Mapping Groundwater Potential Using a Novel Hybrid Intelligence Approach. *Water Resour. Manag.* **2018**, *33*, 281–302. [[CrossRef](#)]
84. Bonham-Carter, G.F. *Geographic Information Systems for Geoscientists: Modeling with GIS*; Pergamon Press: Ottawa, ON, Canada, 1994.
85. Jaafari, A.; Najafi, A.; Pourghasemi, H.R.; Rezaeian, J.; Sattarian, A. GIS-based frequency ratio and index of entropy models for landslide susceptibility assessment in the Caspian forest, northern Iran. *Int. J. Environ. Sci. Technol.* **2014**, *11*, 909–926. [[CrossRef](#)]
86. Ihara, S. *Information Theory for Continuous Systems*; World Scientific Publishing Co. Pte. Ltd.: Singapore, 1993.
87. Massey, D.S.; Nancy, A.D. The Dimensions of Residential. *Soc. Forces* **1988**, *67*, 281–315. [[CrossRef](#)]
88. Yufeng, S.; Fengxiang, J. Landslide Stability Analysis Based on Generalized Information Entropy. In Proceedings of the International Conference on Environmental Science and Information Application Technology, Wuhan, China, 4–5 July 2009.
89. Constantin, M.; Bednarik, M.; Jurchescu, M.C.; Vlaicu, M. Landslide susceptibility assessment using the bivariate statistical analysis and the index of entropy in the Sibiciu Basin (Romania). *Environ. Earth Sci.* **2010**, *63*, 397–406. [[CrossRef](#)]
90. Kumar, P.K.D.; Gopinath, G.; Seralathan, P. Application of remote sensing and GIS for the demarcation of groundwater potential zones of a river basin in Kerala, southwest coast of India. *Int. J. Remote Sens.* **2007**, *28*, 5583–5601. [[CrossRef](#)]
91. El Morjani, Z.E.A. Conception d'un Système D'information à Référence Spatiale Pour la Gestion Environnementale: Application à la Sélection de Sites Potentiels de Stockage de Déchets Ménagers et Industriels en Région Semi-Aride (Souss, Maroc). Ph.D Dissertation, University of Geneva, Geneva, Switzerland, 2002.
92. Heiß, L.; Bouchaou, L.; Reichert, B. Origin and evolution of groundwater in the semi-arid Kerdous Inlier in the Western Anti-Atlas, Morocco. *Grundwasser* **2017**, *23*, 17–28. [[CrossRef](#)]